V.6 Observables at Hadron Colliders

- In hadron colliders, we characterize processes by kinematic variables: transverse momentum p_T, azimuth angle ϕ and pseudorapidity η

$$\eta = -\ln\left(\tan\left[\theta/2\right]\right) \tag{5.49}$$

- For masses much smaller than p_T, pseudorapidity and rapidity are equal

  where rapidity is defined as

$$y = \frac{1}{2}\ln\left(\frac{E+p_{\parallel}}{E-P_{\parallel}}\right) \tag{5.50}$$

- The separation between two objects *i* and *j* in the η–ϕ plane is

$$\Delta R_{i,j} = \sqrt{\left(\eta_i-\eta_j\right)^2+\left(\phi_i-\phi_j\right)^2} \tag{5.51}$$

- Using these variables we define the transverse mass

$$E^2 - p_{\parallel}^2 = m^2 + p_T^2 \equiv m_T^2 \tag{5.52}$$

- Thus,

$$E = m_T \cosh y \tag{5.53}$$

- The maximum value of *y* at fixed E occurs at p_T=0, cosh $y_{max}=\gamma$, yielding y_{max}=7.7 for the Tevatron (2 TeV) and y_{max}=9.6 for LHC (14 TeV)

V.6.1 Observables at Hadron Colliders: Rapidity

- Gluon-gluon scattering is one of the dominant subprocesses in proton-proton collisions

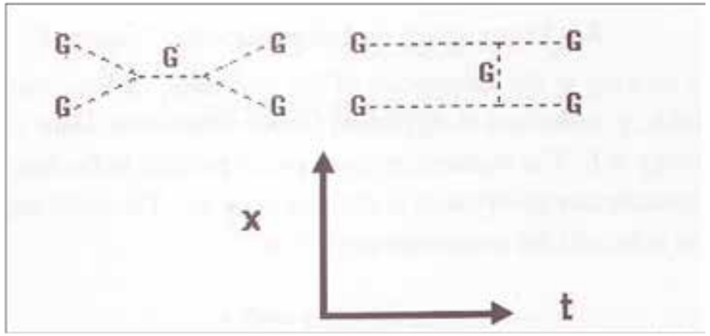

- The rapidity distribution at 14 TeV shows a flat plateau of width $\Delta y = \pm 3$

- This indicates that the produced particles follow single particle phase space at wide angles

- The ATLAS coverage is
  $\Delta y = \pm 2.7$ muon system,
  $\Delta y = \pm 4.9$ em calorimeter
  $\Delta y = \pm 2.5$ tracking

- At the Tevatron at 1.96 TeV the plateau is only $\Delta y = \pm 2$

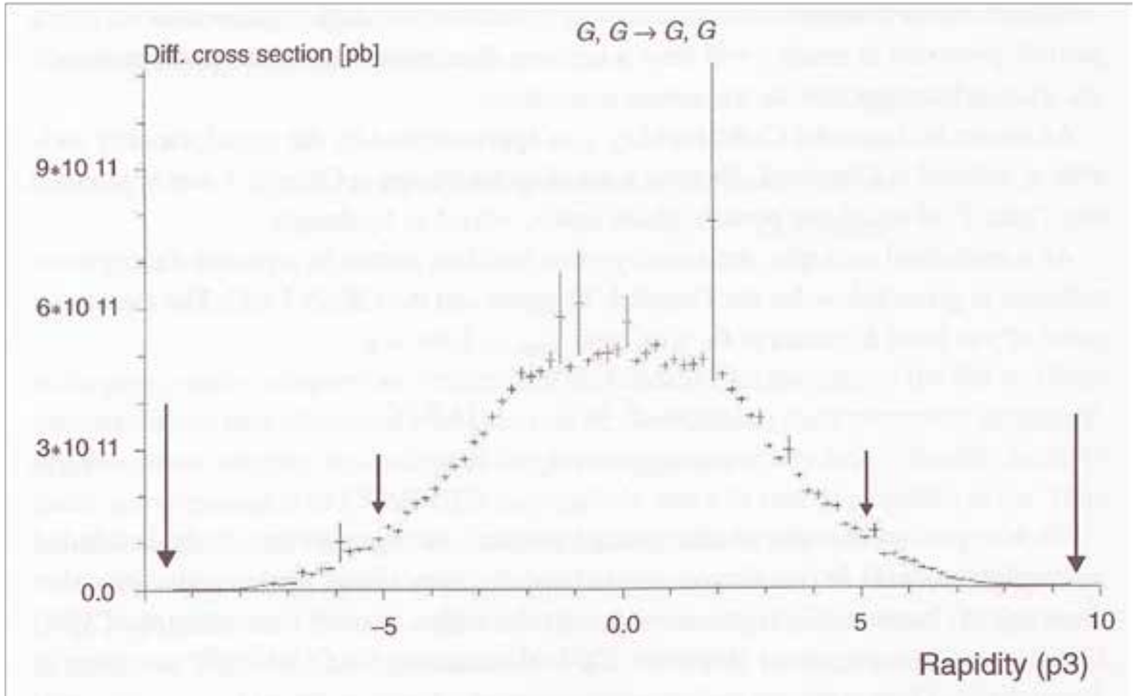

Figure 3.2 Rapidity distribution for produced gluons at the LHC (14 TeV p–p CM energy). The small arrows indicate the limits of the angular coverage of the detector shown in Chapter 2. The larger arrows indicate the initial proton beam rapidity in the CM.

V.6.2 Jet Characteristics

- The jet production cross section depends on η, showing a steeper E_T dependence for large η

- We assume that the p is an incoherent sum of u & d valence quarks, radiated g plus a sea of $q\bar{q}$ pairs

- The reason is that 2 fundamental scales contribute here: the binding energy scale or size of proton and the hard or fundamental collision scale

- We operate at hard scale, $p_T \gg \Lambda_{QCD}$, since p will dissociate into partons with life time $1/\Lambda_{QCD}$ long wrt $1/p_T$
  ➔ incoherent scattering

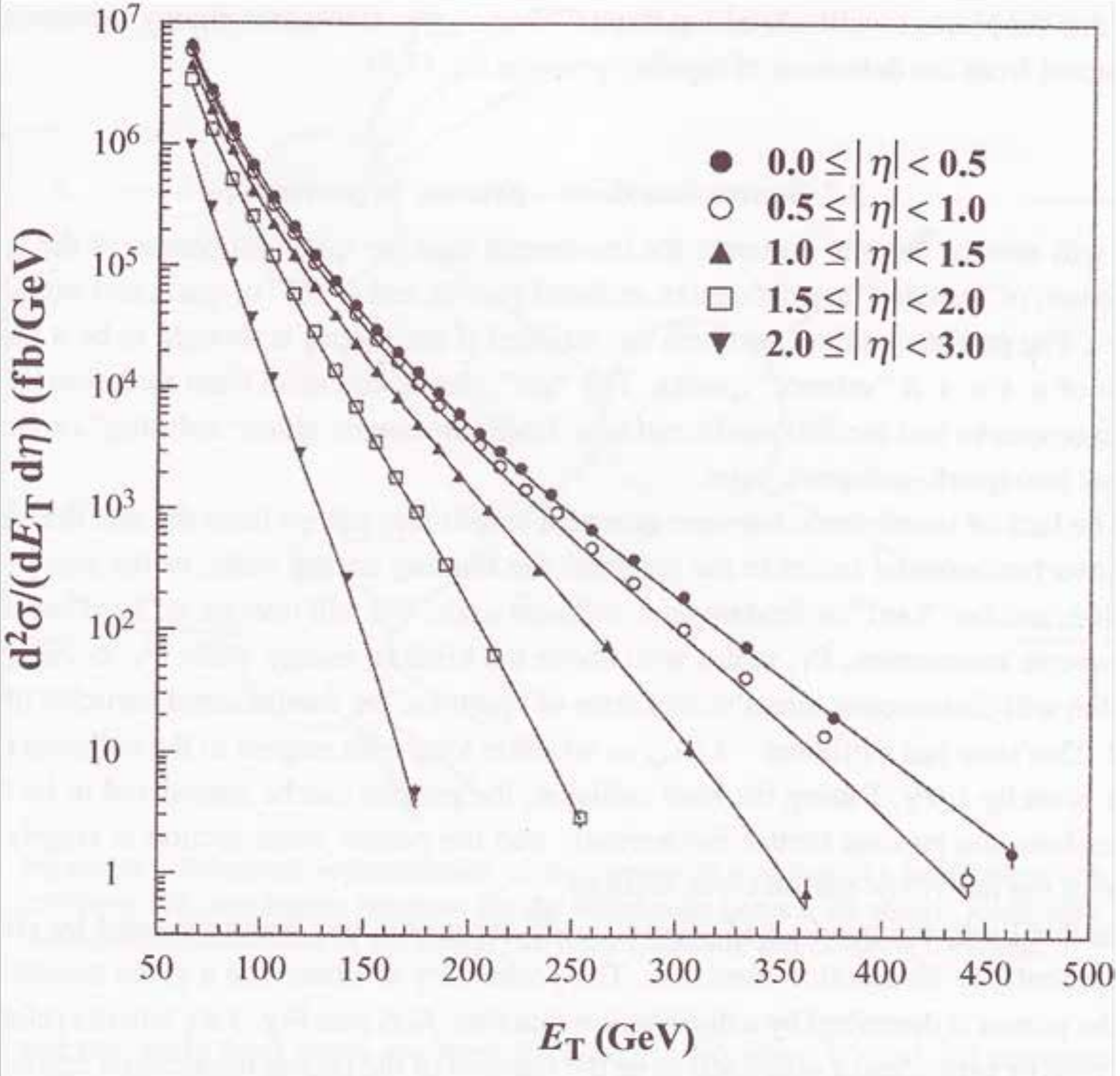

Figure 3.3 D0 data for the jet cross section in different pseudorapidity ranges as a function of transverse energy of the jet ([1] – with permission). The lines represent different distribution function fits.

V.6.2 Jet Characteristics

- ❐ Inclusive jet double differential cross section from ATLAS at 13 TeV

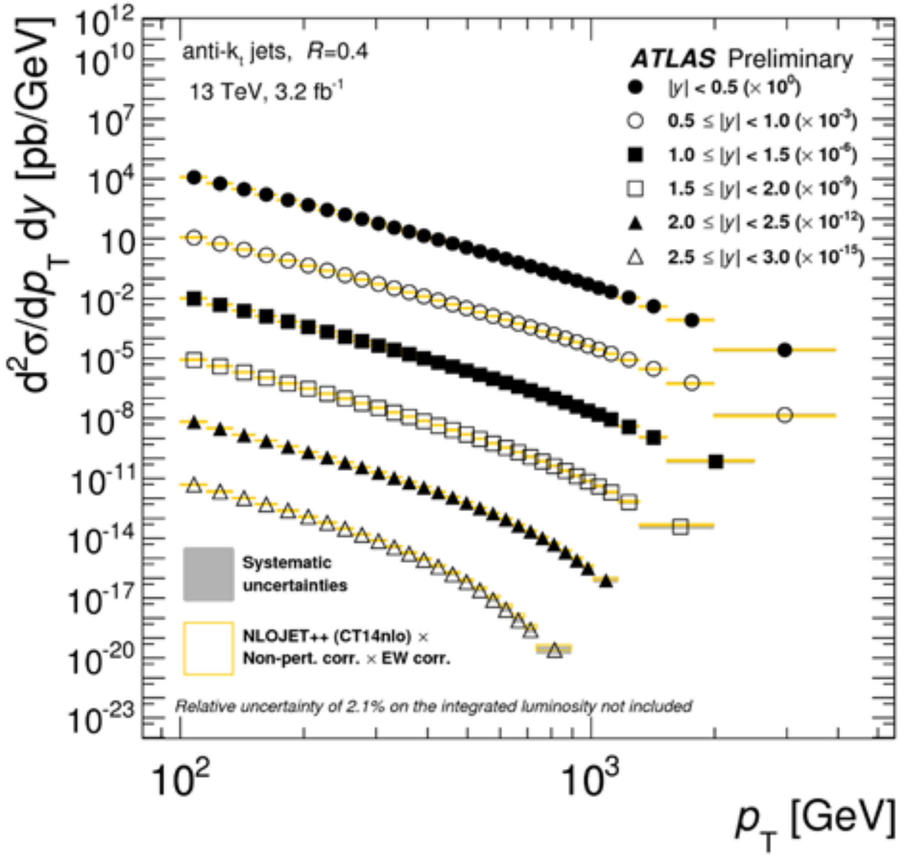

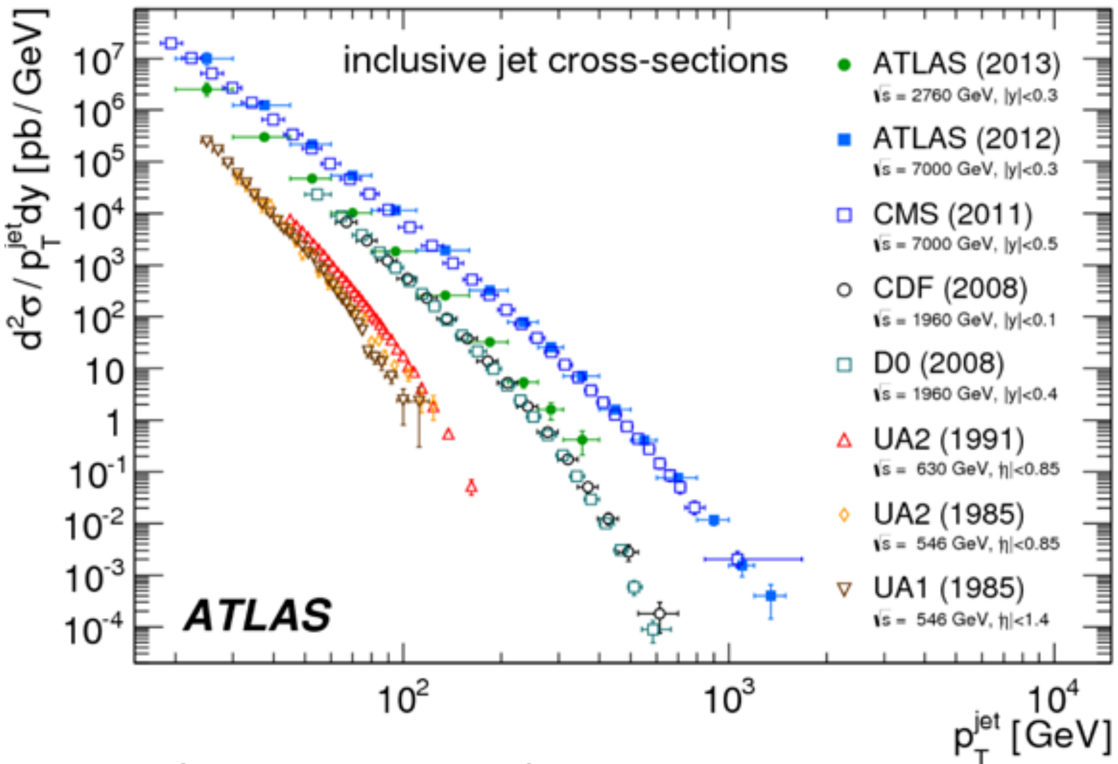

- ❐ Comparison of inclusive jet double differential cross sections from different experiments at different energies

- ❐ At large η, the differential cross section falls off faster at high p_T; At low p_T slopes are similar for different η

- ❐ Data are well described by prediction

V.6.2 Jet Characteristics

- In hadron-hadron collisions typically two partons interact and remaining partons produce the **U**nderlying **E**vent
- They evolve into soft pions (p_T~0.4 GeV) with a charge density of 6 per unit rapidity in a ratio of $\pi^{\pm}:\pi^0$=2:1
- Every interaction will contain a similar distribution of "soft" or low transverse momentum particles, called minimum bias events
- A clear plateau in η is visible rising slowly with √*s*; its width increases with √*s*
- The p_T distribution is tightly localized to values < 0.5 GeV and √s dependence for p_T < 1 GeV is small
- We can fit the p_T behavior with

$$\frac{d^3\sigma}{\pi dy dp_T^2} \sim \frac{A}{(p_T + p_0)^n} \qquad (5.54)$$

A~450 mb/GeV², p_0~1.3 GeV, n~8.2

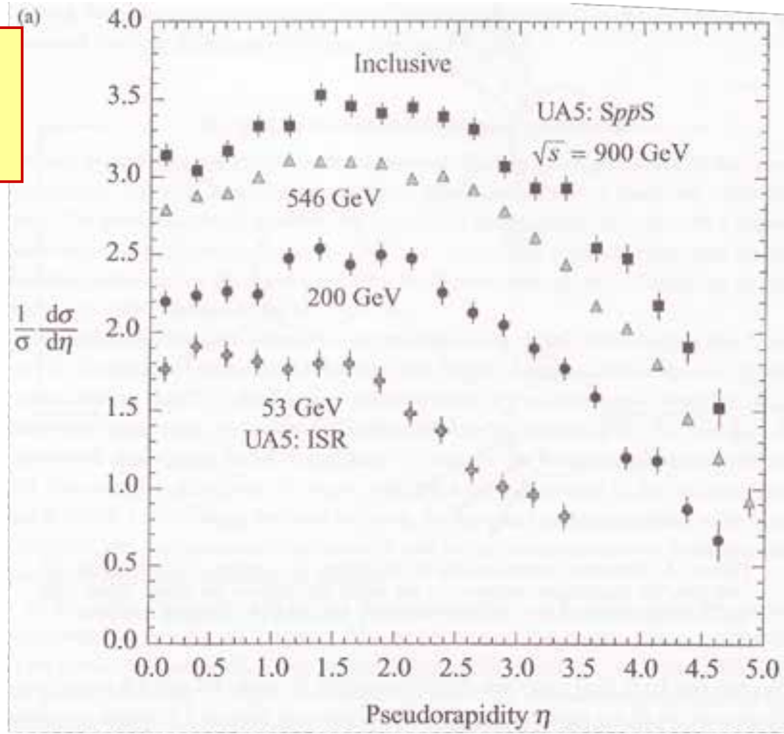

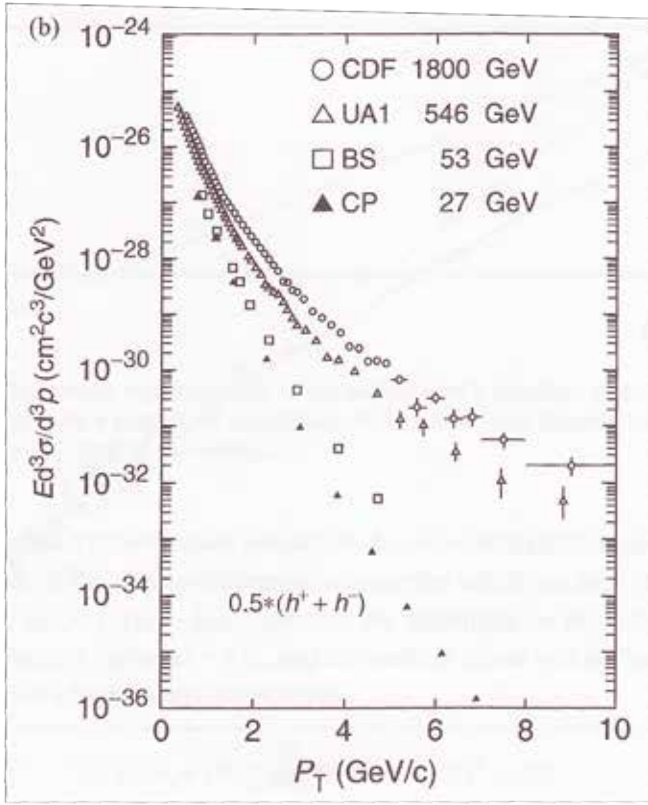

V.6.2 Jet Characteristics

- The coefficient A is of $\mathcal{O}$(100 mb)
  ➔ since this is of the order of total inelastic cross section; the low p_T particles make the bulk of particles produced in inelastic p-p interactions

- For p_T »p_0 cross section drops as p_T^n, large n

- The fragments of hadrons A and B at low p_T merge smoothly with fragmentation products of minijets for p_T > 10 GeV

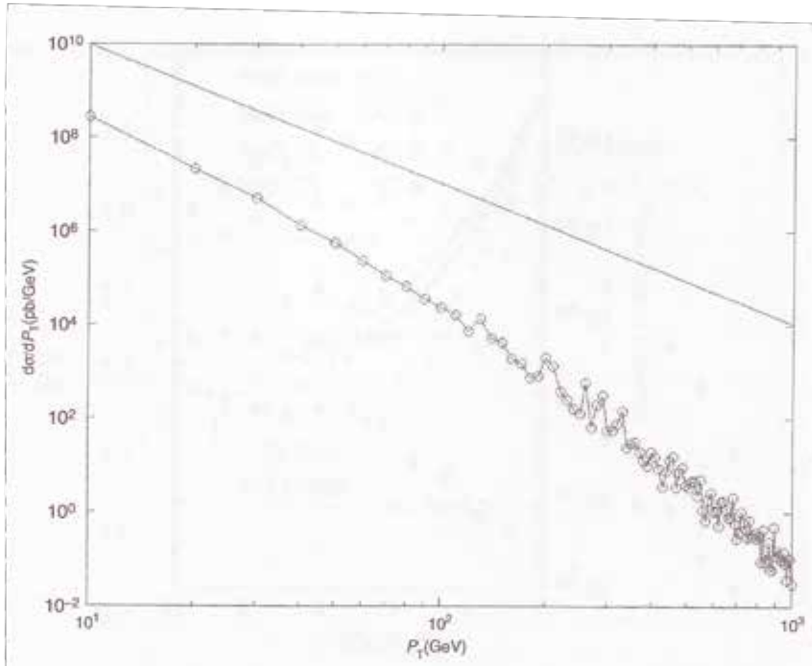

Figure 3.6 COMPHEP Monte Carlo results for the cross section for gluon "jet" production at the LHC at low transverse momentum. The additional solid line indicates a fundamental cross section, which decreases with transverse momenta as the inverse cube, $d\sigma/dP_T \sim 1/P_T^3$.

- Production of g jets has cross section of ~1 mb at p_T ~10 GeV

- Boundary between soft and hard physics is not very definite

- Simulation shows expected cross section for g-g scattering at the LHC at 14 TeV

V.6.3 Distribution Functions

- Thus, quarks and gluons inside proton can be represented by classical distribution functions $f^A_i(x)$, where x is momentum fraction

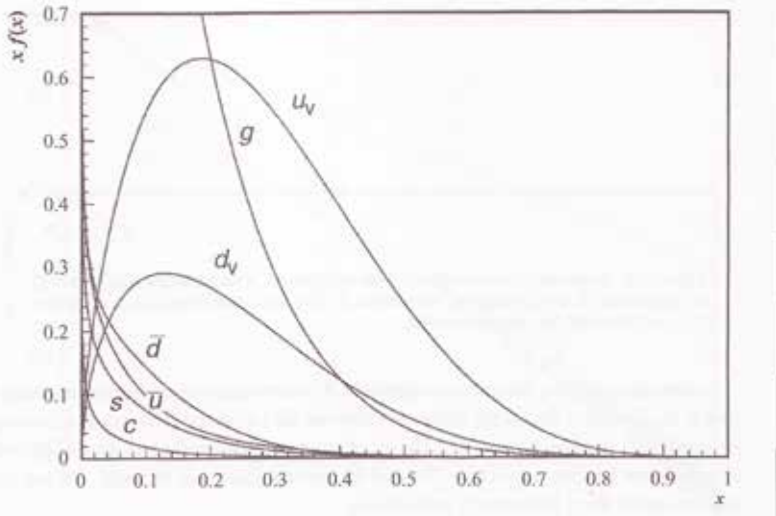

Figure 3.9 Distribution of the momentum fraction of the valence up quarks, gluons, valence down quarks, and "sea" antiquarks in a proton ([4] – with permission). The curves are fits at a fixed momentum transfer scale (see Appendix D).

- If we had only 3 valence quarks their distribution functions would be expected to peak at x=1/3

- Since u &d quark masses are 5 MeV compared to m_p=940 MeV, quark motion is relativistic
  → radiated gluons which have small x distribution

Parton functions

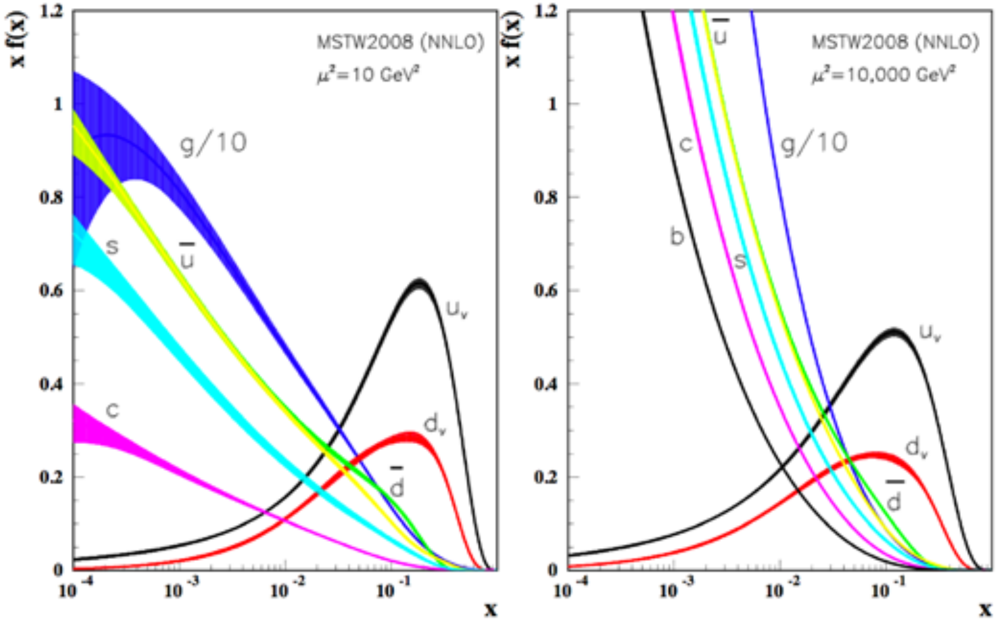

- The gluons themselves can split or decay to $q\bar{q}$, thus apart from $u\bar{u}$, $d\bar{d}$, also $s\bar{s}$ and $c\bar{c}$ pairs may be created at very small x

$$\int_0^1 dx\, u_v(x) = 2, \quad \int_0^1 dx\, d_v(x) = 1 \qquad (5.55)$$

V.6.3 Distribution Functions

- We note that valence and sea quarks carry half the momentum

$$\sum_q \int_0^1 dx\ x\left(q(x)+\bar{q}(x)\right) \simeq 0.5 \qquad (5.56)$$

- The other half is carried by gluons

$$\int_0^1 dx\ x \cdot g(x) \simeq 0.5 \qquad (5.57)$$

- This is confirmed experimentally in lepton scattering experiments

- Suppression at high x is ensured by

$$xg(x) = \tfrac{7}{2}(1-x)^6 \qquad (5.58)$$

- The pointlike cross section for pointlike scattering of partons is

$$\hat{\sigma} \sim \pi\alpha_1\alpha_2 \frac{|A|^2}{\hat{s}} \qquad (5.59)$$

where α_1 and α_2 are the couplings at the 2 vertices and the amplitudes for the various processes are shown in the table below

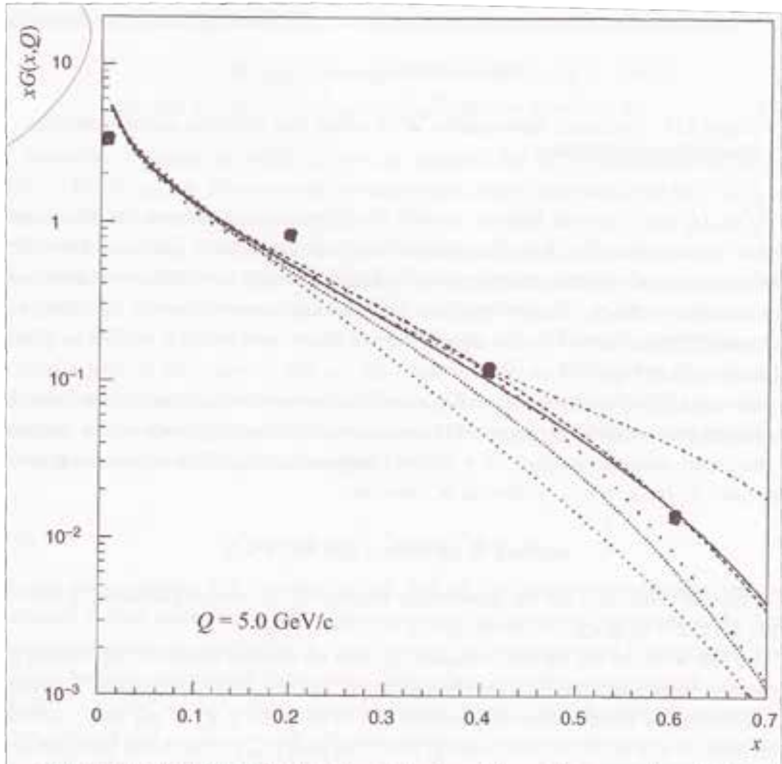

Figure 3.10 Gluon distribution functions taken from different fits to experimental data, shown as lines. The circles are a few points from Eq. (3.5) ([5] – with permission).

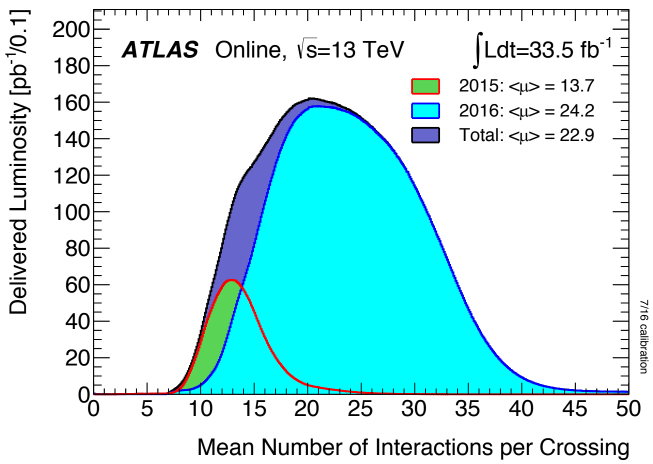

V.6.4 Pointlike Scattering of Partons

- For $\mathcal{L}$~10^{34}/(cm^2 s) & σ~100 mb at the LHC, total inelastic rate is $\sigma \cdot L$~1GHz
  ➔ for 25 ns beam Xing expect 25 minimum bias events/Xing
- g-g scattering has by far the largest cross section (>5 times)
- While final-state particles like e, μ, γ appear directly in the detector, quarks and gluons appear as jets

Table 3.1 *Point like cross sections for parton–parton scattering. The entries have the generic dependence of Eq. (3.10) already factored out. At large transverse momenta, or scattering angles near 90 degrees ($y \sim 0$), the remaining factors are dimensionless numbers of order one ([4] – with permission).* (there should be a ˆ on s, t, u)

Process	$\|A\|^2$	Value at $\theta = \pi/2$
$q+q' \to q+q'$	$\frac{4}{9}[s^2+u^2]/t^2$	2.22
$q+q \to q+q$	$\frac{4}{9}[(s^2+u^2)/t^2+(s^2+t^2)/u^2]-\frac{8}{27}(s^2/ut)$	3.26
$q+\bar{q} \to q'+\bar{q}'$	$\frac{4}{9}[t^2+u^2]/s^2$	0.22
$q+\bar{q} \to q+\bar{q}$	$\frac{4}{9}[(s^2+u^2)/t^2+(t^2+u^2)/s^2]-\frac{8}{27}(u^2/st)$	2.59
$q+\bar{q} \to g+g$	$\frac{32}{27}[t^2+u^2]/tu-\frac{8}{3}[t^2+u^2]/s^2$	1.04
$g+g \to q+\bar{q}$	$\frac{1}{6}[t^2+u^2]/tu-\frac{3}{8}[t^2+u^2]/s^2$	0.15
$g+q \to g+q$	$-\frac{4}{9}[s^2+u^2]/su+[u^2+s^2]/t^2$	6.11
$g+g \to g+g$	$\frac{9}{2}[3-tu/s^2-su/t^2-st/u^2]$	30.4
$q+\bar{q} \to \gamma+g$	$\frac{8}{9}[t^2+u^2]/tu$	
$g+q \to \gamma+q$	$-\frac{1}{3}[s^2+u^2]/su$	

- The process from parton to jets is called fragmentation ➔ it is a complex process simulated in various computer programs (PYTHIA, HERWEG, ISAJET)

V.6.5 Jet Fragmentation

- ❒ Assume fragmentation properties factorize ➔ parent quark or gluon fragment is independent of the mechanism parent is created ➔ we need only a single unified description of fragmentation process

- ❒ # particles in jet depends logarithmically on parent particle momentum

- ❒ Assume: all fragments are pions (simplicity)

- ❒ Assume: p_T acquired in the fragmentation process is limited to the fragment momentum transverse to parent jet axis, $k_T \sim \Lambda_{QCD}$

- ❒ The fragmentation function $D(z)$ describes the distribution in $z=k/P$ of those products in which z is the momentum fraction of the parent with momentum P, carried off by the fragment with momentum k

- ❒ The fraction z is bounded by $M_\pi / P < z < 1$

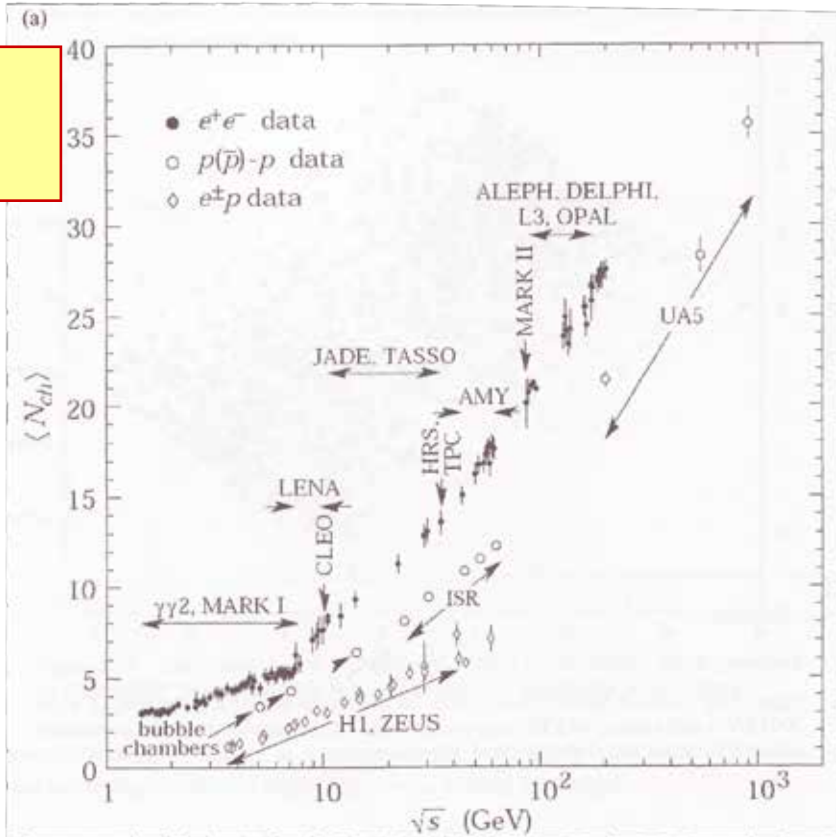

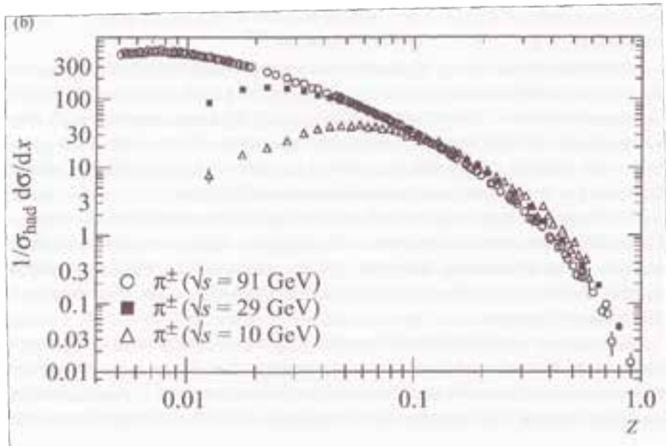

Figure 3.33 Fragmentation of a jet in electron–positron annihilations into an ensemble of final state hadrons. (a) Multiplicity of charged hadrons as a function of the energy of the e^+e^-, p-$(\bar{p})p$, ep initial states. (b) Momentum fraction of the produced pions with respect to the initial electron momentum ([3] – with permission).

V.6.5 Jet Fragmentation

- It has a radiative form similar to that already assumed for the parton distribution functions

- We get $zD(z) = a(1-z)^{\alpha}$ (5.60)

  from which we determine the multiplicity

$$\langle n \rangle = \int D(z)dz \sim a \int_{M_\pi/P}^{1} dz/z \sim a\ln(P/M_\pi) \quad (5.61)$$

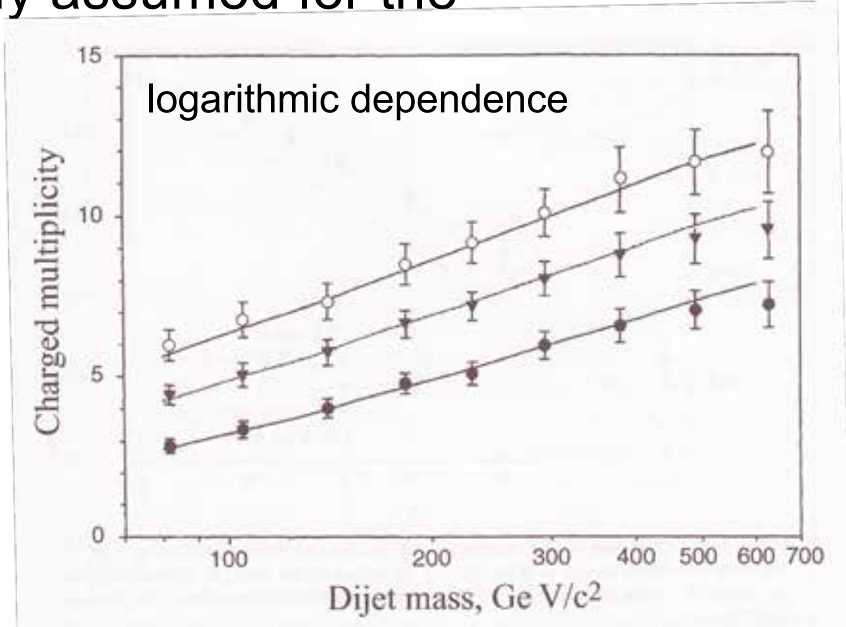

Figure 3.34 CDF data on the mean multiplicity of charged particles within a jet as a function of the mass of the jet–jet system. Note the semi-logarithmic scale. Data for different cone sizes about the jet axis (closed circle, $R = 0.17$; triangle, $R = 0.28$; open circle, $R = 0.47$) are shown ([12] – with permission). The lines are Monte Carlo predictions.

- The fragmentation process implies that we observe a jet of particles that moves approximately along the direction of the parent quark or gluon

- We expect a core within the jet that carries most of the jet momentum and that is localized at a small cone radius, *R*, in (η, ϕ) space

$$R = \sqrt{\Delta\eta^2 + \Delta\phi^2} \quad (5.62)$$

V.6.5 Jet Fragmentation

- The core is surrounded at larger R by many low-energy particles
- From the CDF data it is evident that a sharply peaked distribution of particles around the jet axis exists, as the multiplicity increases less than linear
- In the CDF plot shown on RH side we see 40% of the energy of the jet contained in a cone with R=0.1, while 80% is contained in a cone with R=0.4
- In simulations of the data using $zD(z)=(1-z)^5$ and $\langle k_T \rangle \sim 0.72$ GeV the highest jet energy is about 1/4 of the jet momentum
- Fragmentation is soft introducing non-perturbative effects

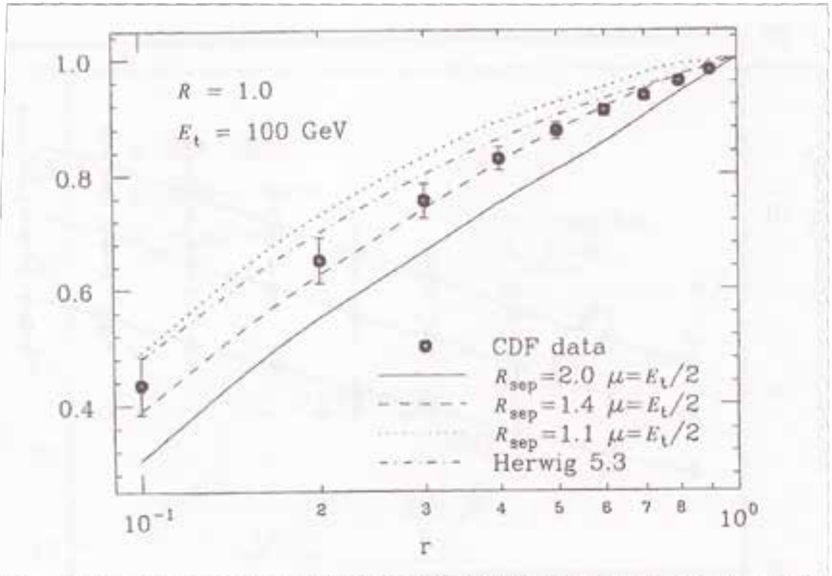

Figure 3.35 CDF data on the distribution of the charged energy fraction of a jet of 100 GeV transverse energy as a function of the radius of the cone, R, surrounding the jet axis ([7] – with permission). The lines correspond to different fits to jet finding algorithms.

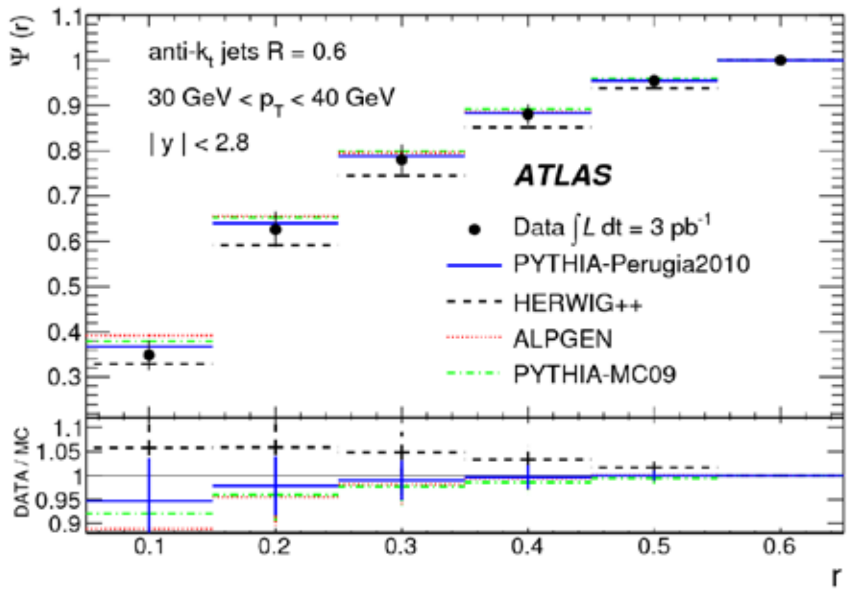

V.6.2 Event Shape Observables

- In pp collisions we have to deal with the **U**nderlying **E**vent since typically 2 partons interact and the remaining partons form the UE (jets)
- Event shape variables are used to separate signal from backgrounds
- Lets look at common event shape variable in $Z^0 \rightarrow \mu^+\mu^-$
  - number of charged tracks ➔ multiplicity increases with dimuon p_T
  - Scalar sum of p_T :
    ➔ increases with dimuon p_T, long tail
  - Beam thrust:
    ➔ increases with dimuon p_T, long tail

$$\sum_i \left|\hat{p}_T^i\right| = \sum p_T \qquad (5.63)$$

$$\mathcal{B} = \sum_i p_T^i \exp[-|\eta_i|] \qquad (5.64)$$

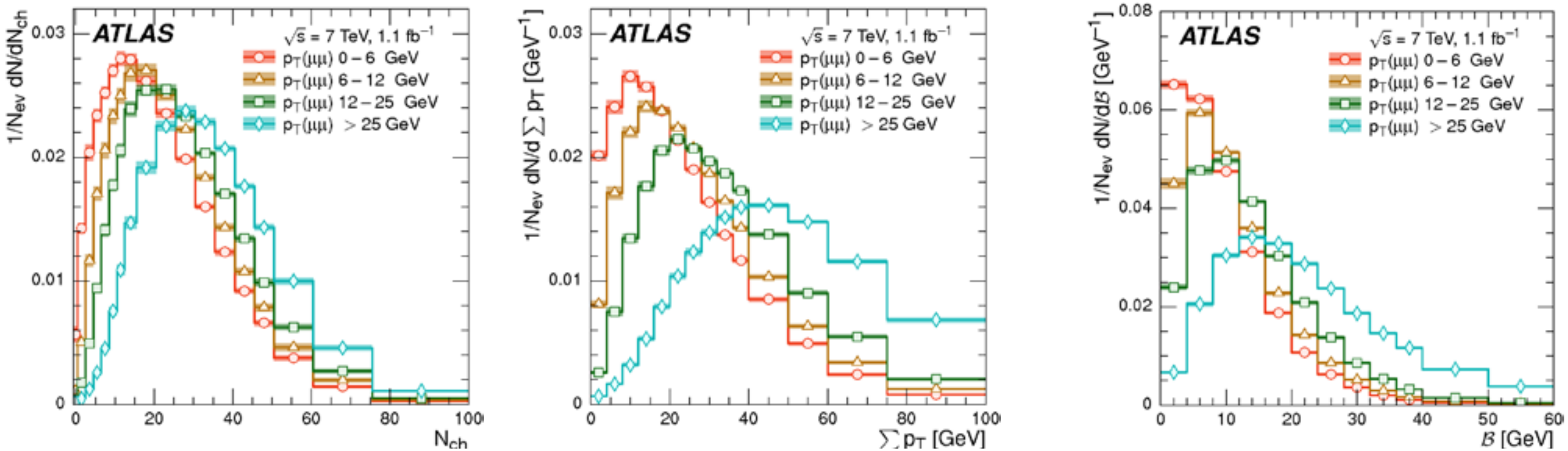

V.6.2 Event Shape Observables

- Thrust:
  ➔ increases with dimuon p_T

$$\mathcal{T} = \max_{\hat{n}_T} \frac{\sum_i \left|\vec{p}_T^{\,i} \cdot \hat{n}_T\right|}{\sum_i \left|\vec{p}_T^{\,i}\right|} \qquad (5.65)$$

$$\mathcal{S} = \frac{\pi^2}{4} \min_{\vec{n}=(n_x,n_y,0)^T} \left(\frac{\sum_i \left|\vec{p}_T^{\,i} \times \vec{n}\right|}{\sum_i \left|p_T^{\,i}\right|} \right)^2 \qquad (5.66)$$

- Spherocity:
  ➔ becomes more symmetric with larger dimuon p_T
- *F* parameter is defined as ratio of smaller to larger eigenvalues of the transverse momentum tensor

❒ For high dimuon p_T different prediction yield reasonable description

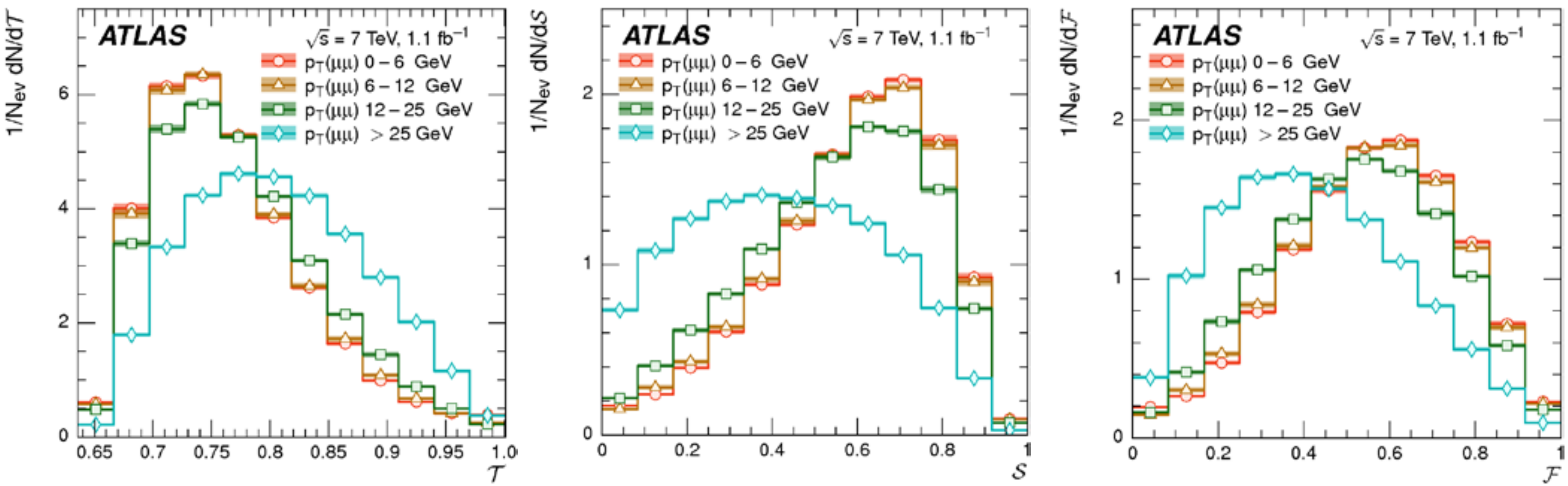

VI. Weak Boson Production and Decay

VI.1 *W*-Decays

- The discovery of weak bosons at the CERN SPS $p\bar{p}$ collider by UA1/UA2 gave spectacular support to the SM as it was predicted by EW gauge theory

- The weak bosons are detected by their decays

- In the SM *W* and *Z* bosons decay through their fundamental gauge couplings to basic quarks and leptons

- W bosons were first detected in their leptonic mode $W \to e\bar{\nu}_e$

- The amplitude for $W^- \to e^- \bar{\nu}_e$ is

$$M = -i\frac{g}{\sqrt{2}}\varepsilon_\mu^\lambda(p)\bar{u}(p_e)\gamma^\mu \frac{1}{2}(1-\gamma_5)v(k) \qquad (6.1)$$

  where g is the charged-current weak coupling

- Averaging $|M|^2$ over the W polarizations and summing over fermions, we get in the massless e & ν approximations:

$$\frac{1}{3}\sum_{\text{spin}}|M|^2 = \frac{g^2}{6}\left(-g^{\mu\nu} + \frac{p^\mu p^\nu}{M_W^2}\right)Tr\left(\not{p}_e\gamma_\mu \not{k}\gamma_\nu \tfrac{1}{2}(1-\gamma_5)\right) = \frac{1}{3}g^2 M_W^2 \qquad (6.2)$$

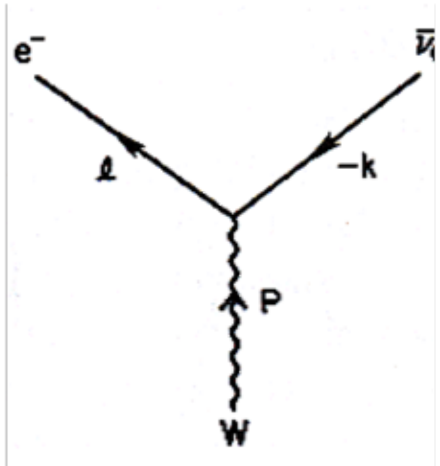

Fig. 8.1. Leptonic decay mode $W^- \to e^-\bar{\nu}_e$.

VI.1 *W*-Decays

- Hence, the differential decay rate in *W* rest frame is

$$d\Gamma(W \to e\nu) = \frac{1}{2M_W}\left(\frac{1}{3}g^2M_W^2\right)\frac{1}{(2\pi)^2}d_2(LIPS) \qquad (6.3)$$

- We can choose the gauge boson polarization vectors as

$$\varepsilon_0^\mu = \left(\frac{P}{M_W},0,0,\frac{E}{M_W}\right)$$ longitudinal (h=0) (6.4)

$$\varepsilon_\pm^\mu = \frac{1}{\sqrt{2}}\left(0,1,\pm i,0\right)$$ transverse (h=$\pm$1) (6.5)

- We then obtain the decay distribution of *e* in *W* rest frame, which are

$$d\Gamma_0(W \to e\nu) \sim \sin^2\hat{\theta} \qquad (6.6)$$

$$d\Gamma_\pm(W \to e\nu) \sim \left(1 \pm \cos\hat{\theta}\right)^2 \qquad (6.7)$$

where $\hat{\theta}$ is the angle of the *e* with respect to the longitudinal axis

- The phase space integral is $$\int d_2(LIPS) = \frac{1}{2}\pi\int\frac{d\Omega}{4\pi} = \frac{1}{2}\pi \qquad (6.8)$$

VI.1 *W*-Decays

yielding a partial decay width of

$$\Gamma(W^- \to e^- \bar{\nu}) = \frac{1}{48\pi} g^2 M_W = \frac{G_F}{\sqrt{2}} \frac{M_W^3}{6\pi} \equiv \Gamma_W^0 \qquad (6.9)$$

- Since $g^2 = 8M^2_W G_F/\sqrt{2}$ & $M_W = 80.1$ GeV we obtain

$$\Gamma_W^0 = 0.225\ GeV \qquad (6.10)$$

- Decays to $\mu\nu$ & $\tau\nu$ yield same width if lepton masses are neglected
- We also approximate the total hadronic decay rate by that to $q\bar{q}$' assuming that the latter fragment into hadrons with probability 1
- Thus, neglecting also quark masses we get

$$\Gamma(W^- \to e^- \bar{\nu}) = \Gamma(W^- \to \mu^- \bar{\nu}) = \Gamma(W^- \to \tau^- \bar{\nu}) \equiv \Gamma_W^0 \qquad (6.11)$$

$$\Gamma(W^- \to q\bar{q}') = 3|V_{qq'}|^2 \Gamma_W^0 \qquad (6.12)$$

where $V_{qq'}$ is the CKM *ME* and factor of 3 results from color

- Summing over all quark families N_F yields

$$\sum_{q,q'} |V_{qq'}|^2 = \sum_{q'} 1 = N_F = 2 \qquad (6.13)$$

VI.1 *W*-Decays

- So, the total hadronic width in the massless fermion approximation is

$$\Gamma(W \to hadrons) \simeq 3N_F \Gamma(W \to leptons) \simeq 6\Gamma_W^0 = 1.35\ GeV \tag{6.14}$$

and the total width is approximately

$$\Gamma(W \to all) \simeq 9\Gamma_W^0 = 2.1\ GeV \tag{6.15}$$

$$\Gamma_{tot}^{exp} = (2.124 \pm 0.041)\ GeV \tag{6.16}$$

- This translates into a mean lifetime of $\tau = 2\times10^{-25}$ s
- The branching fraction for $W^- \to e^-\bar{\nu}_e$

$$\mathcal{B}(W^- \to e^-\bar{\nu}) \simeq \frac{\Gamma(W^- \to e^-\bar{\nu})}{\Gamma(W^- \to all)} \simeq \frac{1}{9} \tag{6.17}$$

- We expect dominant contributions from $W^- \to u\bar{d}$ and $W^- \to c\bar{s}$, since

$$|V_{ud}| \approx |V_{cs}| \approx 1 \tag{6.18}$$

- First-order QCD corrections modify hadronic widths by $1+\alpha_s(M_W)/\pi$ with $\alpha_s(M_W)=0.12$, yielding $\Gamma_{tot}=2.08$ GeV

VI.1 *W*-Decays

- The partial widths are

decay	partial width	$\mathcal{B}_{th}$[%]	$\mathcal{B}_{exp}$ [%]
$W\rightarrow e\bar{\nu}_e$	0.225 GeV	10.8	10.68 ± 0.12
$W\rightarrow \mu\bar{\nu}_\mu$	0.225 GeV	10.8	10.72 ± 0.16
$W\rightarrow \tau\bar{\nu}_\tau$	0.225 GeV	10.8	10.57 ± 0.22
$W\rightarrow u\bar{d}$	0.666 GeV	32.1	
$W\rightarrow c\bar{s}$	0.664 GeV	32.0	
$W\rightarrow u\bar{s}$	0.035 GeV	1.7	67.96 ± 0.35
$W\rightarrow c\bar{d}$	0.035 GeV	1.7	
$W\rightarrow c\bar{b}$	0.001 GeV	0.5	
$W\rightarrow u\bar{b}$	0.00001GeV	0.005	

- For leptons we observe universality as expected by the SM

VI.2 Z^0-Decays

- The Z^0 was first detected through $Z^0 \to e^+e^-$ (CERN)
- The amplitude for this mode is

$$M = -ig_Z \varepsilon_\mu^\lambda(p)\bar{u}(p_{e^-})\gamma^m(g_V + g_A\gamma_5)v(p_{e^+}) \tag{6.19}$$

- Following the same procedure we used for the $W \to e^-\bar{\nu}_e$ decay, we get the partial width

$$\Gamma(Z^0 \to e^+e^-) = \frac{1}{48\pi}\left(2\sqrt{2}g_Z\right)^2\left(\frac{g_V^2 + g_A^2}{2}\right)M_Z \tag{6.20}$$

- Substituting $g^2_Z = 8G_F M^2_Z/\sqrt{2}$ yields

$$\Gamma(Z^0 \to e^+e^-) = \frac{8G_F^2 M_Z^3}{12\pi\sqrt{2}}\left(g_V^2 + g_A^2\right) = 8\left(g_V^2 + g_A^2\right)\Gamma_Z^0 \tag{6.21}$$

- In the massless fermion approximation similar expressions hold $\ell\bar{\ell}$ and $q\bar{q}$ partial widths

$$\Gamma(Z^0 \to e^+e^-) = 8\left((g_V^\ell)^2 + (g_A^\ell)^2\right)\Gamma_Z^0 \tag{6.22}$$

$$\Gamma(Z^0 \to q\bar{q}) = 24\left((g_V^q)^2 + (g_A^q)^2\right)\Gamma_Z^0 \tag{6.23}$$

with $\ell = e, \nu_e, \mu, \nu_\mu, \tau, \nu_\tau$ and $q = u, d, s, c, b$

VI.2 Z^0-Decays

- Note the color factor between $\ell\bar{\ell}$ and $q\bar{q}$ modes
- Appropriate g_V and g_A must be used in each case
- Recall the SM couplings

$$g_V^f = \frac{1}{2}T_3^f - Q^f x_W \qquad \& \qquad g_A^f = -\frac{1}{2}T_3^f \tag{6.24}$$

and hence

$$\left(g_V^f\right)^2 + \left(g_A^f\right)^2 = \frac{1}{2}\left(T_3^f\right)^2 - T_3^f Q^f x_W + \left(Q^f\right)^2 x_W^2 = \frac{1}{8}\left(1 - 4\left|Q^f\right| x_W + 8(Q^f)^2 x_W^2\right) \tag{6.25}$$

- For x_W=0.23 and M_Z=91.19 GeV we obtain the lowest-order partial widths

$$\Gamma(Z^0 \to \nu_e \bar{\nu}_e) = \Gamma_Z^0 = 0.17\ GeV \tag{6.26}$$

$$\Gamma(Z^0 \to e^+ e^-) = \Gamma_Z^0\left(1 - 4x_W + 8x_W^2\right) = 0.08\ GeV \tag{6.27}$$

$$\Gamma(Z^0 \to u\bar{u}) = 3\Gamma_Z^0\left(1 - \frac{8}{3}x_W + \frac{32}{9}x_W^2\right) = 0.29\ \text{GeV} \tag{6.28}$$

$$\Gamma(Z^0 \to d\bar{d}) = 3\Gamma_Z^0\left(1 - \frac{4}{3}x_W + \frac{8}{9}x_W^2\right) = 0.37\ \text{GeV} \tag{6.29}$$

- Summing over 3 families except for the top quark we get the Z^0 total width in the massless fermion approximation

$$\Gamma_Z = \Gamma_Z^0\left(21 - 40x_W + 160x_W^2\right) = 2.4\ \text{GeV} \tag{6.30}$$

VI.2 Z^0-Decays

- Thus the corresponding Z^0 branching fractions are

$$\mathcal{B}(Z^0 \to \nu_e \bar{\nu}_e) \simeq 0.07 \tag{6.31}$$

$$\mathcal{B}(Z^0 \to e^+ e^-) \simeq 0.03 \tag{6.32}$$

$$\mathcal{B}(Z^0 \to u\bar{u}) \simeq 0.12 \tag{6.33}$$

$$\mathcal{B}(Z^0 \to d\bar{d}) \simeq 0.15 \tag{6.34}$$

- Similar branching fractions are obtained for the corresponding channels of the other families
- First-order QCD corrections to hadronic Z^0 decays are $1+\alpha_s(M_Z)/\pi$ if quark masses are neglected with $\alpha_s(M_Z)=0.12$
- The predicted total width with QCD corrections is $\Gamma(Z^0)=2.49$ GeV while measurements yield $\Gamma_{tot}(Z^0)=2.4952\pm0.0021$ GeV

VI.2 Z^0-Decays

❒ For the individual decay channels partial decay widths and branching fractions are

decay	partial width	$\mathcal{B}_{th}$[%]	$\mathcal{B}_{exp}$ [%]	$\mathcal{B}_{exp}$ [%]
$Z\to\nu_e\bar{\nu}_e$	0.166 GeV	6.7		
$Z\to\nu_\mu\bar{\nu}_\mu$	0.166 GeV	6.7		20.00 ± 0.06
$Z\to\nu_\tau\bar{\nu}_\tau$	0.166 GeV	6.7		
$Z\to e^+e^-$	0.083 GeV	3.4	3.363 ± 0.004	
$Z\to\mu^+\mu^-$	0.083 GeV	3.4	3.366 ± 0.007	
$Z\to\tau^+\tau^-$	0.083 GeV	3.4	3.370 ± 0.008	
$Z\to d\bar{d}$	0.383 GeV	15.4		
$Z\to s\bar{s}$	0.383 GeV	15.4		$3\times15.6\pm0.4$
$Z\to b\bar{b}$	0.378 GeV	15.2	15.13 ± 0.05	
$Z\to u\bar{u}$	0.297 GeV	12.0		$2\times11.6\pm0.6$
$Z\to c\bar{c}$	0.296 GeV	11.9	11.81 ± 0.33	

VI.3 Number of Light Neutrinos

- The partial widths come in ratios of

$$\Gamma_Z(Z^0 \to \nu_e \bar{\nu}_e) : \Gamma_Z(Z^0 \to e^+ e^-) : \Gamma_Z(Z^0 \to u\bar{u}) : \Gamma_Z(Z^0 \to d\bar{d}) = 2.0 : 1.0 : 3.6 : 4.6 \quad (6.35)$$

- The branching fraction into the invisible modes is

$$\mathcal{B}(Z^0 \to \nu_e \bar{\nu}_e + \nu_\mu \bar{\nu}_\mu + \nu_\tau \bar{\nu}_\tau) \simeq 20\% \quad (6.36)$$

- The total width is measured from the resonant line shape of the total e^+e^- cross section near $s=M^2_Z$
- The visible and invisible parts of Γ_Z can be separated using visible cross sections around the Z^0 peak
- Any new particle with non-trivial SU(2)×U(1) QNs will couple to the Z^0, if they are light enough appearing in Z^0 decays thus modifying either Γ_Z^{vis} or Γ_Z^{inv}
- One example is new νs
- Any ν belonging to an SU(2) doublet contributes 0.17 GeV to Γ_Z^{inv}
- The measurements yields 499±1.5 MeV

VI.3 Number of Light Neutrinos

- Using lepton universality and $$\Gamma_Z^{inv} = N_\nu \left(\Gamma_{\nu\nu} / \Gamma_{ee} \right)_{SM} \qquad (6.37)$$

  we obtain for $N_\nu \Gamma_{\nu\nu}/\Gamma_{ee}$=5.942±0.016, which is in good agreement with 3 families of quarks and leptons

- A fit to the Z^0 line shape yields

$$N_\nu = 2.9841 \pm 0.083 \qquad (6.38)$$

- Note that a heavy ν is not ruled out by this measurement

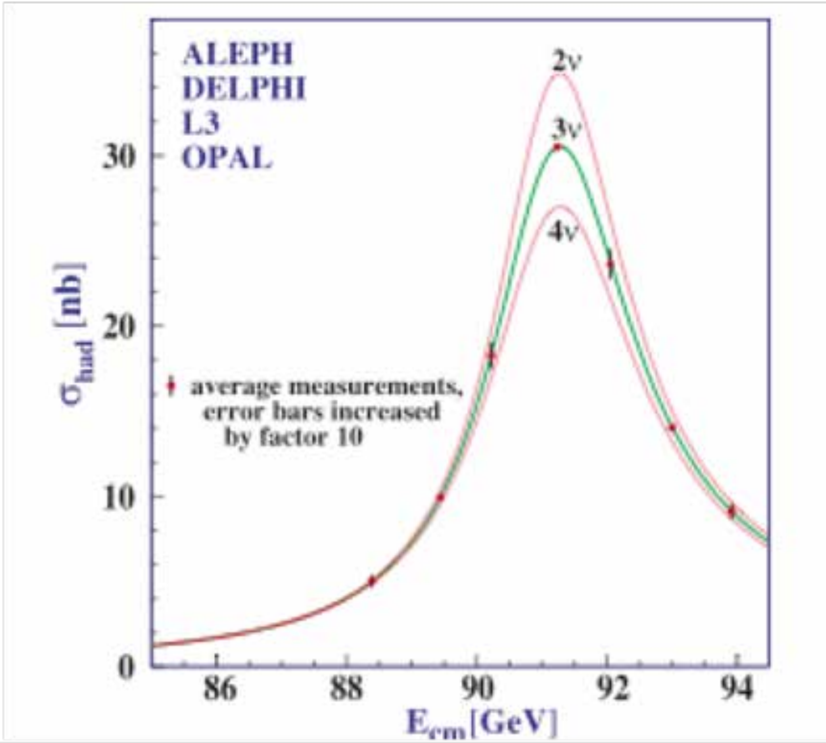

Figure 40.8: Combined data from the ALEPH, DELPHI, L3, and OPAL Collaborations for the cross section in e^+e^- annihilation into hadronic final states as a function of the center-of-mass energy near the Z pole. The curves show the predictions of the Standard Model with two, three, and four species of light neutrinos. The asymmetry of the curve is produced by initial-state radiation. Note that the error bars have been increased by a factor ten for display purposes. References:

VI.4 Gauge Boson Widths

- Hadron collider experiments measure the ratio Γ_Z/Γ_W through

$$R=\frac{\sigma(p\bar{p}\to W^-\to e^-\bar{\nu})}{\sigma(p\bar{p}\to Z^0\to e^+e^-)}=\frac{\sigma(p\bar{p}\to W^-)}{\sigma(p\bar{p}\to Z^0)}\frac{\Gamma(W^-\to e^-\nu_e)}{\Gamma(Z^0\to e^+e^-)}\frac{\Gamma_Z}{\Gamma_W} \quad (6.39)$$

- The ratios $\Gamma(Z^0\to e^+e^-)/\Gamma(W^-\to e^-\nu)$ & σ_W/σ_Z can be calculated rather accurately, since many theoretical uncertainties cancel

- The results are $\sigma_W/\sigma_Z=3.3\pm0.2$ & $\Gamma(Z^0\to e^+e^-)/\Gamma(W^-\to e^-\nu)=0.37\pm0.01$

- With measurements of $R=10.49\pm0.25$ we get

$$\Gamma_Z/\Gamma_W=1.176\pm0.028\pm0.06_{th} \quad (6.40)$$

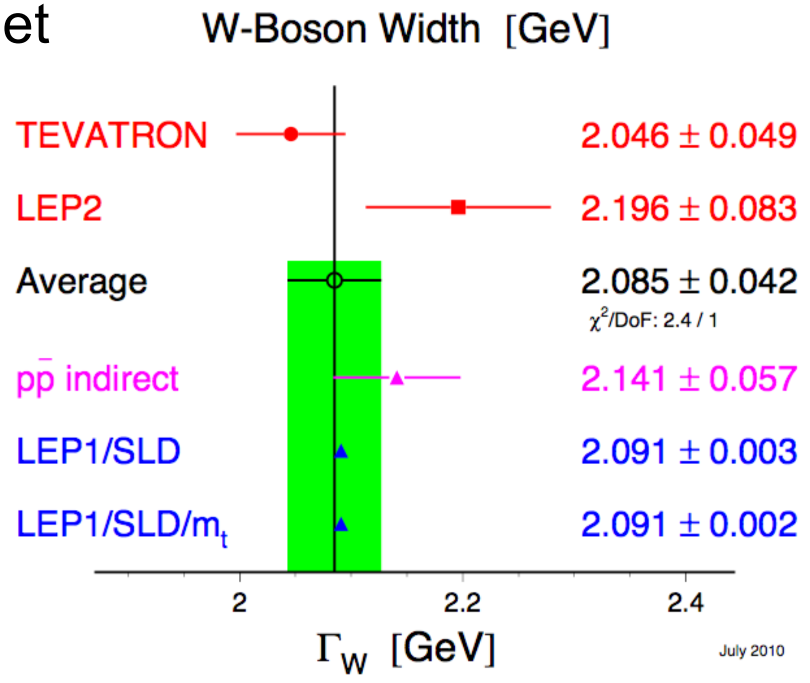

- From precise measurements of Γ_Z/Γ_W, Γ_Z & N_ν we can infer Γ_W

- The most precise measurement of Γ_W comes from the Tevatron

$$\text{Tevatron}: \Gamma_W=2.046\pm0.049 \quad (6.41)$$

- Direct LEP II & Tevatron measurements yield

$$\Gamma_W=2.085\pm0.042\ \text{GeV} \quad (6.42)$$

VI.5 Hadronic $W^{\pm}$-Production

- Hadronic $W^{\pm}$ production $A+B \to W^{\pm}+X$ is based on the quark subprocess $q\bar{q}' \to W^{+}$ and the conjugated process for W^{-}

- The ME is the same as that in $W^{\pm}$ decay

$$M = -iV_{qq'} \frac{g}{\sqrt{2}} \varepsilon_{\mu}^{\lambda *}(k) \bar{v}(p') \gamma^{\mu} \frac{1}{2}(1-\gamma_5) u(p) \tag{6.43}$$

- This yields a subprocess cross section of

$$\hat{\sigma}(q\bar{q}' \to W^{+}) = \left(\frac{1}{2}\right)^2 \frac{1}{2\hat{s}} \left(\left|V_{qq'}\right|^2 \frac{8G_F}{\sqrt{2}} M_W^4 \right) 2\pi \int d(LIPS) \tag{6.44}$$

where $\hat{s} = (p+p')^2$

- The phase space evaluation yields

$$\int \frac{d^3p}{2Ep} \delta(k-p-p') = \delta(\hat{s} - M_W^2) \tag{6.45}$$

and hence

$$\hat{\sigma}(q\bar{q}' \to W^{+}) = 2\pi \left|V_{qq'}\right|^2 \frac{G_F}{\sqrt{2}} M_W^2 \delta(\hat{s} - M_W^2) \tag{6.46}$$

- The total $W^{\pm}$ cross section is obtained by convolving $\hat{\sigma}$ with the quark density distributions $q(x_a, M^2_W)$ & $\bar{q}'(x_b, M^2_W)$ including a color factor of $3\times 1/3 \times 1/3$, where x_a & x_b denote the momentum fractions of q & $\bar{q}'$

VI.5 Hadronic $W^{\pm}$-Production

- $$\sigma(AB \to W^{+}X) = \frac{K}{3}\int_0^1 dx_a \int_0^1 x_b \sum_{q,q'} q(x_a, M_W^2)\bar{q}'(x_b, M_W^2)\hat{\sigma}(q\bar{q}' \to W^{\pm}) \qquad (6.47)$$

- We have assumed that $q^2 = \hat{s} = M_W^2$
- The K-factor includes 1st-order QCD corrections $$K \simeq 1 + \frac{8\pi}{9}\alpha_s(M_W^2) \qquad (6.48)$$
- We transform the integration to $\hat{s}$ & y variables $$dx_a dx_b = \frac{d\hat{s}dy}{s} \qquad (6.49)$$ where $$y = \frac{1}{2}\ln\left(\frac{E+p_L}{E-p_L}\right) \qquad (6.50)$$ is the rapidity of the W-boson in the AB CM frame

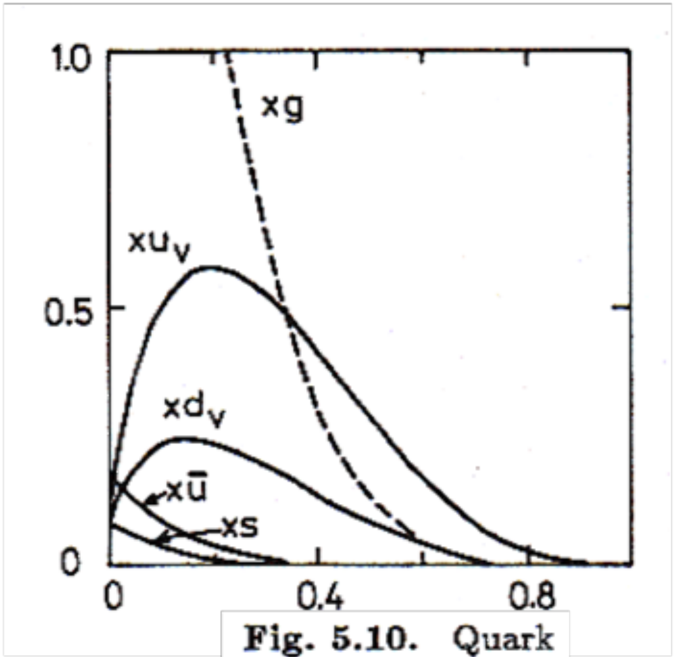

Fig. 5.10. Quark and gluon distributions from parameterization B.

- Note that $s^{1/2}$ is the invariant mass of the AB system while $\hat{s}$ is that of the ab system

VI.5 Hadronic $W^{\pm}$-Production

- The integral over ds takes out the δ function, yielding

$$\frac{d\sigma}{dy}\left(W^{+}\right)=K\frac{2\pi}{3}\frac{G_F}{\sqrt{2}}\sum_{q,q'}\left|V_{qq'}\right|^2 x_a x_b q(x_a,M_W^2)\bar{q}'(x_b,M_W^2) \qquad (6.51)$$

where x_a & x_b are now evaluated at

$$x_a=\frac{M_W}{\sqrt{s}}e^{y},\quad x_b=\frac{M_W}{\sqrt{s}}e^{-y} \qquad (6.52)$$

- For pp scattering, the differential cross section in the Cabibbo-mixing approximation and evaluating all quark distributions at $q^2=M_W^2$ is

$$\frac{d\sigma}{dy}\left(pp\to W^{+}\right)=K\frac{2\pi}{3}\frac{G_F}{\sqrt{2}}x_a x_b\left\{\cos^2\theta_c\left[u(x_a)\bar{d}(x_b)+\bar{d}(x_a)u(x_b)\right]+\sin^2\theta_c\left[u(x_a)\bar{s}(x_b)+\bar{s}(x_a)u(x_b)\right]\right\} \qquad (6.53)$$

- For the SU(3) symmetric sea approximation we have $\bar{u}(x)=\bar{d}(x)=\bar{s}(x)$

- Here the differential cross section simplifies to

$$\frac{d\sigma}{dy}\left(pp\to W^{+}\right)=K\frac{2\pi}{3}\frac{G_F}{\sqrt{2}}x_a x_b\left\{u(x_a)\bar{d}(x_b)+\bar{d}(x_a)u(x_b)\right\} \qquad (6.54)$$

- For $p\bar{p}$ collisions the $W^{\pm}$ differential cross section is

$$\frac{d\sigma}{dy}\left(p\bar{p}\to W^{+}\right)=K\frac{2\pi}{3}\frac{G_F}{\sqrt{2}}x_a x_b\left\{\cos^2\theta_c\left[u(x_a)d(x_b)+\bar{d}(x_a)\bar{u}(x_b)\right]+\sin^2\theta_c\left[u(x_a)s(x_b)+\bar{s}(x_a)\bar{u}(x_b)\right]\right\} \qquad (6.55)$$

VI.5 Hadronic $W^{\pm}$-Production

- In the valence dominance approximation for low CM energies this becomes

$$\frac{d\sigma}{dy}\left(p\bar{p}\rightarrow W^{+}X\right)\simeq K\frac{2\pi}{3}\frac{G_{F}}{\sqrt{2}}x_{a}x_{b}\left\{u(x_{a})d(x_{b})\right\} \qquad (6.56)$$

- The total cross sections are obtained by integration over y

- ATLAS measured (13 TeV)

$$\sigma(pp\rightarrow W^{+}X\rightarrow e^{+}\nu X)=20639.3\pm 24.4_{stat}\pm 555.6_{sys}\pm 433.4_{lum}\ \mathrm{pb} \qquad (6.57)$$

- CDF measured (1.96 TeV)

$$\sigma(p\bar{p}\rightarrow W^{-}X\rightarrow e^{-}\bar{\nu}_{e}X)= 2740\pm 10_{stat}\,53_{sys}\pm 165\ \mathrm{pb} \qquad (6.58)$$

- UA1 measured (0.63 TeV)

$$\sigma(p\bar{p}\rightarrow W^{-}X\rightarrow e^{-}\bar{\nu}_{e}X)= 630\pm 40_{stat}\,100_{sys}\ \mathrm{pb} \qquad (6.59)$$

- All measurements are in good agreement with the NNLO prediction

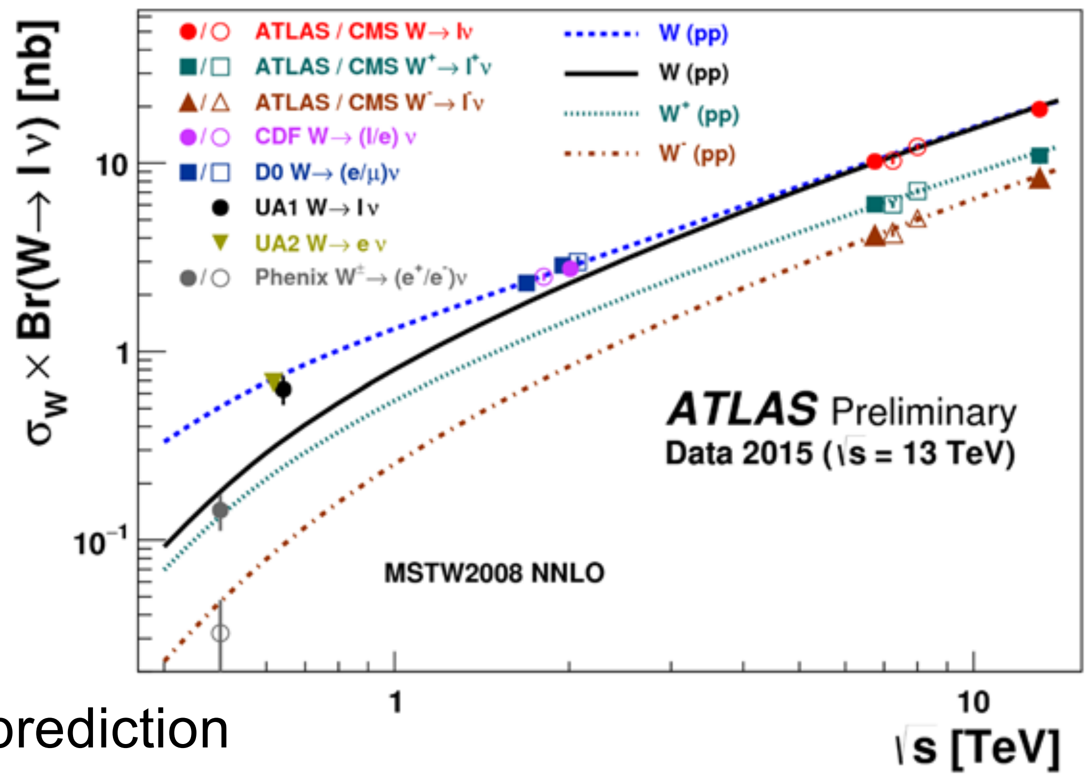

VI.6 Hadronic Z^0-Production

- The calculation of the cross section for $AB \to Z^0 X$ is similar to that of $W^\pm$ production

- The ME squared for the fusion subprocess $q\bar{q} \to Z^0$ is

$$|M|^2 = \left(2\sqrt{2}g_Z\right)^2 M_Z^2 \frac{\left[\left(g_V^q\right)^2 + \left(g_A^q\right)^2\right]}{2} = 32\frac{G_F}{\sqrt{2}} M_Z^4 \left[\left(g_V^q\right)^2 + \left(g_A^q\right)^2\right] \tag{6.60}$$

- The subprocess cross section & resulting color-averaged hadronic cross sections are

$$\hat{\sigma}(q\bar{q} \to Z^0) = 8\pi \frac{G_F}{\sqrt{2}} M_Z^2 \left[\left(g_V^q\right)^2 + \left(g_A^q\right)^2\right] \delta(\hat{s} - M_Z^2) \tag{6.61}$$

$$\frac{d\sigma}{dy}(AB \to Z^0 X) = K \frac{8\pi}{3} \frac{G_F}{\sqrt{2}} M_Z^2 \sum_q \left[\left(g_V^q\right)^2 + \left(g_A^q\right)^2\right] x_a x_b q(x_a) \bar{q}(x_b) \tag{6.62}$$

- For Z^0 production in $p\bar{p}$ & pp collisions, $d\sigma/dy$ is

$$\begin{aligned}\frac{d\sigma}{dy}(p\bar{p} \to Z^0 X) = K \frac{\pi}{3} \frac{G_F}{\sqrt{2}} x_a x_b & \left\{\left[1 - \frac{8}{3}x_W + \frac{32}{9}x_W^2\right]\left[u(x_a)u(x_b) + \bar{u}(x_a)\bar{u}(x_b)\right]\right. \\ & \left. + \left[1 - \frac{4}{3}x_W + \frac{8}{9}x_W^2\right]\left[d(x_a)d(x_b) + \bar{d}(x_a)\bar{d}(x_b) + s(x_a)s(x_b) + \bar{s}(x_a)\bar{s}(x_b)\right]\right\}\end{aligned} \tag{6.63}$$

VI.6 Hadronic Z^0-Production

$$\frac{d\sigma}{dy}(pp \to Z^0X) = K\frac{\pi}{3}\frac{G_F}{\sqrt{2}}x_a x_b \left\{\left[1-\frac{8}{3}x_W+\frac{32}{9}x_W^2\right]\left[u(x_a)\bar{u}(x_b)+\bar{u}(x_a)u(x_b)\right]\right.$$
$$\left.+\left[1-\frac{4}{3}x_W+\frac{8}{9}x_W^2\right]\left[d(x_a)\bar{d}(x_b)+\bar{d}(x_a)d(x_b)+s(x_a)\bar{s}(x_b)+\bar{s}(x_a)s(x_b)\right]\right\} \quad (6.64)$$

- ATLAS measured (13 TeV) $\sigma(pp \to Z^0X \to e^+e^-X) = 1981.2 \pm 7.0_{stat} \pm 38.1_{sys} \pm 41.6_{lum}$ pb (6.65)

- CDF measured (1.96 TeV)

$$\sigma(p\bar{p} \to Z^0X \to e^+e^-X) = 253.9 \pm 3.3_{stat} \pm 4.6_{sys} \pm 15.2_{lum} \text{ pb} \quad (6.66)$$

- UA1 measured

$$\sigma(p\bar{p} \to Z^0X \to e^+e^-X) = 71 \pm 7_{stat} \pm 11_{sys} \text{ pb} \quad (6.67)$$

- All measurements agree well with the NNLO prediction

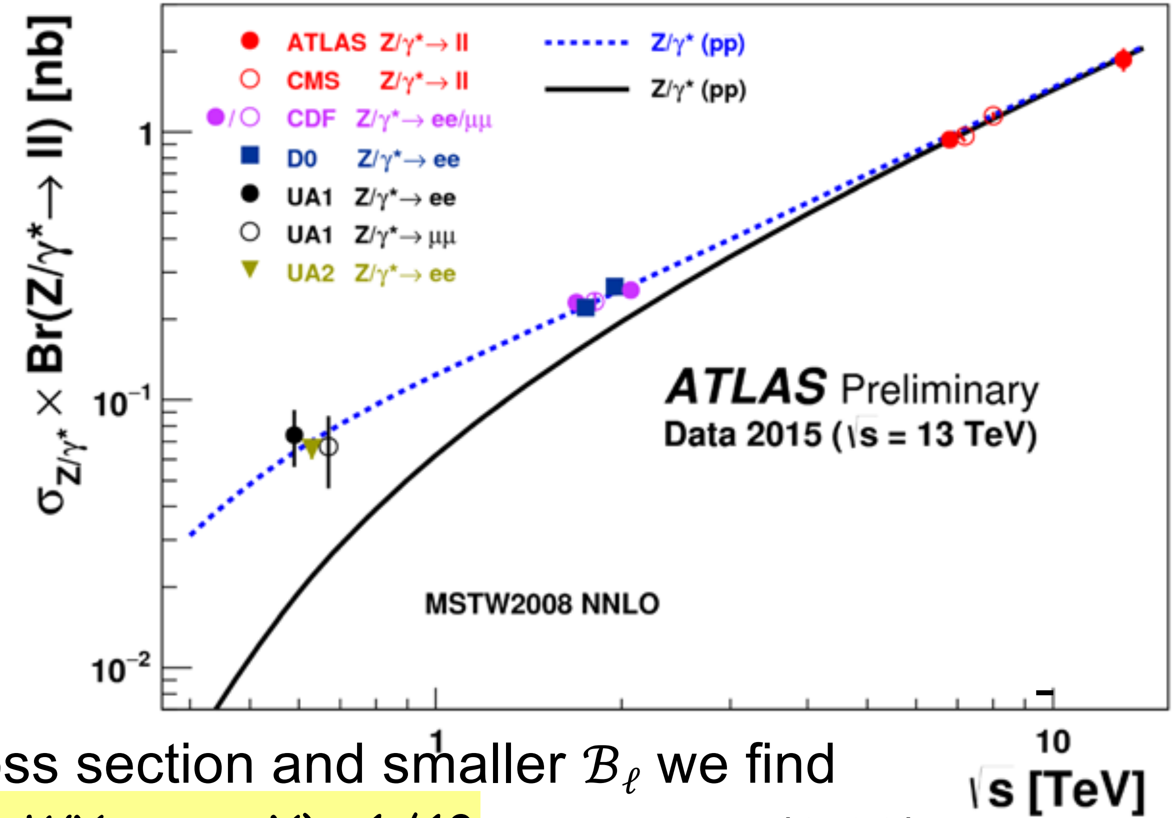

- Due to smaller production cross section and smaller $\mathcal{B}_\ell$ we find

$$\sigma(p\bar{p} \to Z^0X \to e^+e^-X) / \sigma(p\bar{p} \to WX \to e^-\bar{\nu}_e X) \simeq 1/10 \quad (6.68)$$

VI.7 Hadronic $W \to e\nu$ Production

- Lets examine the distribution of $W \to e\nu$ in more detail
- We must calculate the complete production & decay subprocess

  $u\bar{d} \to W^+ \to e^+\nu_e$

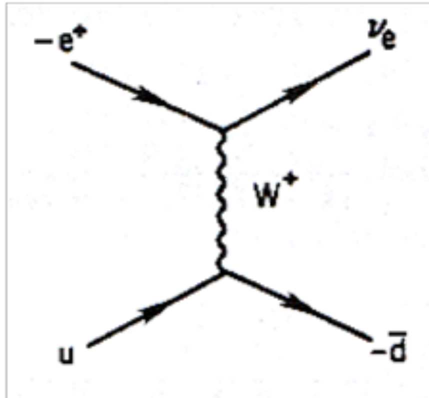

- The spin-averaged differential cross section is

$$\frac{d\hat{\sigma}}{d\cos\hat{\theta}}(u\bar{d} \to e^+\nu) = \frac{|V_{ud}|^2}{8\pi}\left(\frac{G_F M_W^2}{\sqrt{2}}\right)^2 \frac{\hat{s}(1+\cos\hat{\theta})^2}{(\hat{s}-M_W^2)^2+(\Gamma_W M_W)^2} \qquad (6.69)$$

where we have neglected quark & lepton masses

- Integration over $\cos\hat{\theta}$ yields

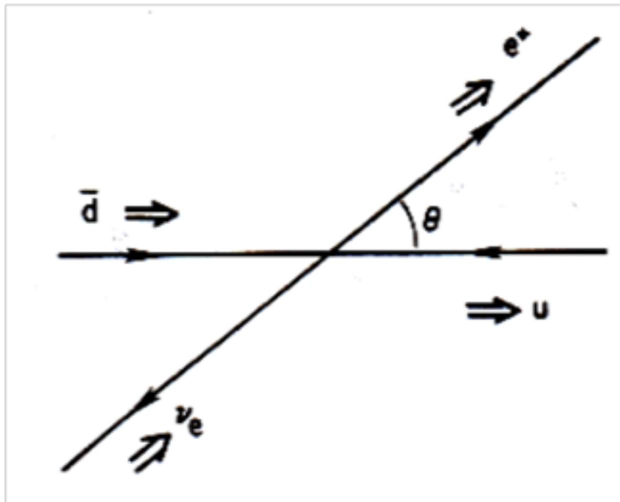

$$\hat{\sigma}(u\bar{d} \to e^+\nu) = \frac{|V_{ud}|^2}{3\pi}\left(\frac{G_F M_W^2}{\sqrt{2}}\right)^2 \frac{\hat{s}}{(\hat{s}-M_W^2)^2+(\Gamma_W M_W)^2} \qquad (6.70)$$

- $d\hat{\sigma}/d\cos\hat{\theta}$ vanishes at $\cos\hat{\theta}$=-1, being a consequence of helicity conservation (m_e=0) in collinear scattering

- Hence, the e^+ is preferentially emitted along the $\bar{d}$ direction

VI.7 Hadronic $W \to e\nu$ Production

- In $p\bar{p}$ collisions below $s^{1/2}$=1 TeV, $\bar{p}$ is the main source of $\bar{d}$ quark, while p is that of u quark
- Thus, the e^+ is preferentially produced in the hemisphere of $\bar{p}$ beam direction
- The inclusive hadronic cross section for $AB \to e\nu X$ has the form

$$d\sigma(AB \to e^+\nu X) = \tfrac{1}{3}\sum_{q,q'}\int_0^1 dx_a \int_0^1 dx_b\, q(x_a)\bar{q}'(x_b)\, d\hat{\sigma}(q\bar{q}' \to e^+\nu_e) \qquad (6.71)$$

Color

- The parton distributions are evolved up to $s=M^2_W$
- Note that eqn (6.71) is sufficient for choosing x_a, x_b and $\cos\hat{\theta}$
- The e-rapidity in the $u\bar{d}$ CM frame is defined by

$$\hat{y} = \frac{1}{2}\ln\left[\frac{\hat{E}_e + \hat{p}_e^L}{\hat{E}_e - \hat{p}_e^L}\right] = \ln\cot\left(\frac{1}{2}\hat{\theta}\right) \qquad (6.72)$$

- Thus

$$\frac{d\hat{\sigma}}{d\hat{y}} = \sin^2\hat{\theta}\,\frac{d\hat{\sigma}}{d\cos\hat{\theta}} \simeq \left(\frac{1+\tanh\hat{y}}{\cos\hat{y}}\right)^2 \qquad (6.73)$$

VI.7 Hadronic $W\rightarrow e\nu$ Production

- The e laboratory momentum and rapidity are related x_a, x_b & $\hat{\theta}$ by

$$E_e = \frac{1}{4}\sqrt{s}\left[x_a(1+\cos\hat{\theta}) + x_b(1-\cos\hat{\theta})\right] \tag{6.74}$$

$$p_e^L = \frac{1}{4}\sqrt{s}\left[x_a(1+\cos\hat{\theta}) - x_b(1-\cos\hat{\theta})\right] \tag{6.75}$$

$$y = \frac{1}{2}\ln\left[\frac{x_a(1+\cos\hat{\theta})}{x_b(1-\cos\hat{\theta})}\right] = \frac{1}{2}\ln\left(\frac{x_a}{x_b}\right) + \hat{y} \tag{6.76}$$

- Hence the *e*-lab rapidity distribution has the form

$$\frac{d\sigma}{dy}\left(AB\rightarrow eX\right) = \frac{1}{3}\sum_{q,q'}\int_0^1 dx_a \int_0^1 dx_b q(x_a)\bar{q}'(x_b)\left[\frac{d\hat{\sigma}}{d\cos\hat{\theta}}\left(q\bar{q}'\rightarrow e\nu\right)\sin^2\hat{\theta}\right] \tag{6.77}$$

- The [ ] is evaluated at $\hat{y}=y-1/2\ln(x_a/x_b)$ with $\cos\hat{\theta}=\tanh\hat{y}$

- The transverse momentum distribution of the *e* & ν are important in the identification of $W\rightarrow e\nu$ events

- In the $u\bar{d}\rightarrow e\nu$ subprocess CM frame, the transverse momentum $\hat{p}_T$ of the *e* & ν are back-to-back and have the same magnitude

$$\hat{p}_T^2 = \tfrac{1}{4}\hat{s}\sin^2\hat{\theta} = \hat{t}\hat{u}/\hat{s} \tag{6.78}$$

VI.7 Hadronic $W \to e\nu$ Production

- Changing variable from $\cos\hat{\theta}$ to $d\hat{p}^2_T$ using $\cos\hat{\theta} = [1-4\,\hat{p}_T{}^2/\hat{s}]^{1/2}$ we encounter the Jacobian

$$\frac{d\cos\hat{\theta}}{d\hat{p}_T^2} = -\frac{2}{3}\left(1-\frac{4\hat{p}_T^2}{\hat{s}}\right)^{-\frac{1}{2}} = -\frac{2}{\hat{s}\cos\hat{\theta}} \qquad (6.79)$$

- Since angles $\hat{\theta}$ and π-$\hat{\theta}$ contribute to the same $\hat{p}_T$, terms linear in $\cos\hat{\theta}$ in the differential cross section cancel yielding

$$\frac{d\hat{\sigma}}{d\hat{p}_T^2} = \hat{\sigma}\frac{3}{2}\frac{\left(1+\cos^2\hat{\theta}\right)}{\hat{s}\left|\cos\hat{\theta}\right|} = \frac{\hat{\sigma}}{\hat{s}}3\frac{1-2\hat{p}_T^2/\hat{s}}{\left(1-4\hat{p}_T^2/\hat{s}\right)^{\frac{1}{2}}} \qquad (6.80)$$

- The divergence at $\hat{\theta} = 1/2\pi$ (upper endpoint $\hat{p}_T = (1/2)\,\hat{s}^{1/2} = (1/2)M_W$ of the $\hat{p}_T$ distribution stems from Jacobian factor and is known as Jacobian peak (characteristic of all 2-body modes)

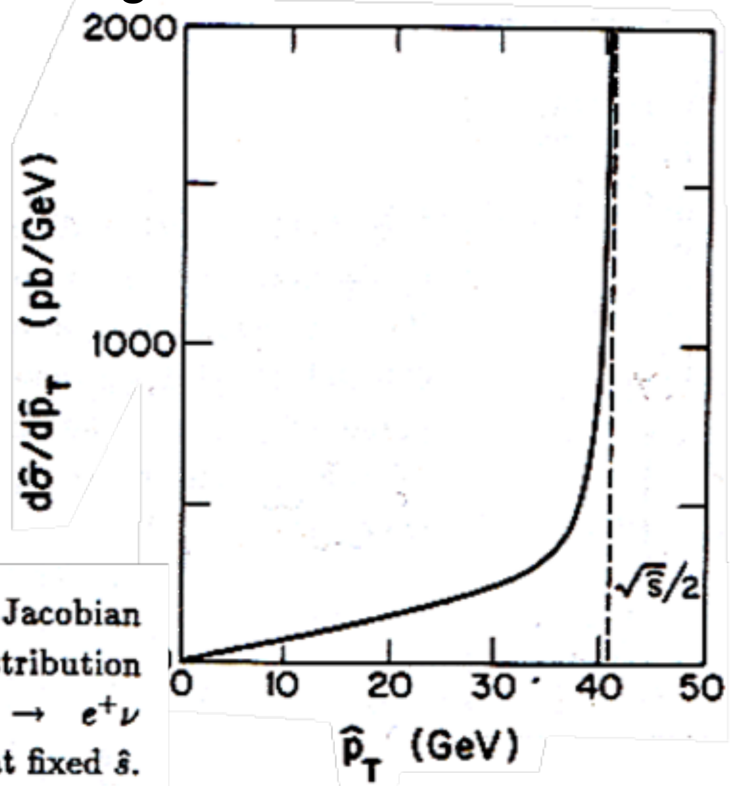

Fig. 8.9. Jacobian peak p_T-distribution in the $u\bar{d} \to e^+\nu$ subprocess at fixed $\hat{s}$.

VI.7 Hadronic $W\rightarrow e\nu$ Production

- Consider simply lowest-order subprocess $q\bar{q}' \rightarrow W \rightarrow e\nu$ ➔ incident quarks are longitudinal ➔ W boson is produced longitudinally & laboratory transverse momentum of e is subprocess transverse momentum $\hat{p}_T = p_T$

- Here, the p_T distribution is obtained by convolving $d\hat{\sigma}/d\hat{p}_T^2$ with the quark distributions averaged only over the Breit-Wigner $\hat{s}$ dependence of $\hat{\sigma}(q\bar{q}\rightarrow e\nu)$

- Integration over s removes the singularity and leaves the Jacobian peak of finite height near $p_T = M_W/2$

- Higher-order subprocesses, such as $u\bar{d} \rightarrow W^+ g$, give the W a transverse momentum distribution that smears out the Jacobian peak in the p_{eT} distribution

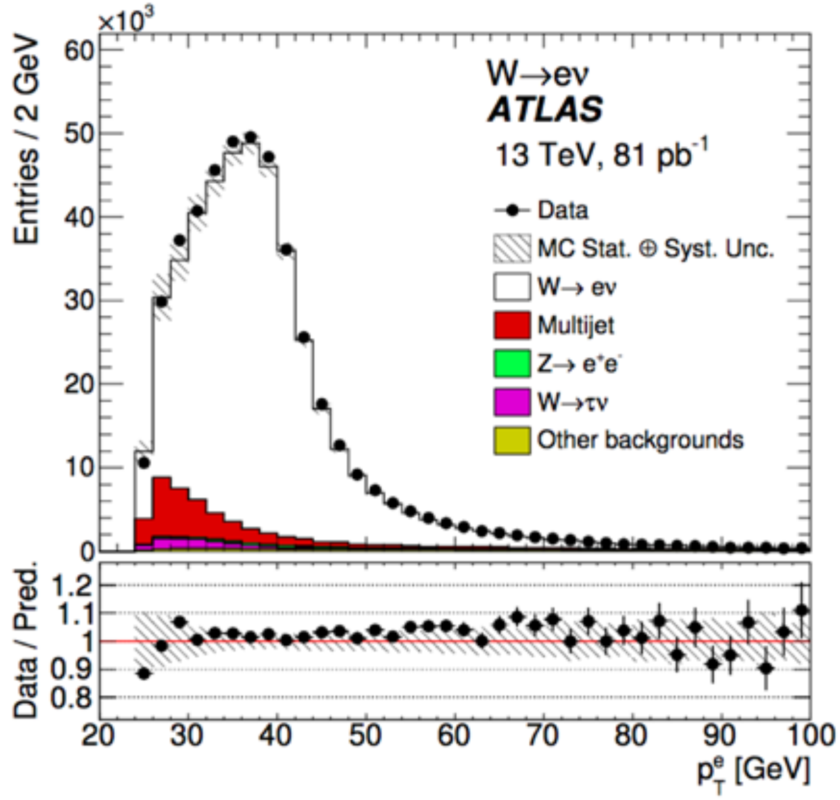

VI.7 Hadronic $W \to e\nu$ Production

- This smearing makes it difficult to obtain an accurate determination of M_W from the p_{eT} distribution alone
- It is possible, however, to exploit information about the ν momentum
- Since all hadrons and charged leptons with sizable p_T are detected the overall p_T imbalance for detected particles gives approximate measure of the undetected ν transverse momentum $p_{\nu T}$
- One cannot make a similar determination of the longitudinal momentum component $p_{\nu L}$, since particles can escape down the beam pipe
- Another quantity that has a sharp Jacobian peak is the transverse mass

VI.8 Transverse Mass

- The $e\nu$ transverse mass $m_T(e, \nu)$ is defined by

$$m_T^2(e,\nu) = \left(\left|\vec{p}_e^{\,T}\right| + \left|\vec{p}_\nu^{\,T}\right|\right)^2 - \left(\vec{p}_e^{\,T} + \vec{p}_\nu^{\,T}\right)^2 = 2\left|\vec{p}_e^{\,T}\right| E_{miss}^T \left(1 - \cos\phi_{e-\nu}\right) \tag{6.81}$$

- Comparing this to the invariant mass yields

$$0 \le m^2(e,\nu) - m_T^2(e,\nu) = 2\left[\sqrt{\left((p_e^T)^2 + (p_e^L)^2\right)}\sqrt{\left((p_\nu^T)^2 + (p_\nu^L)^2\right)} - \left|p_e^T\right|\left|p_\nu^T\right| - \left|p_e^L\right|\left|p_\nu^L\right|\right] \tag{6.82}$$

- Thus, $m_T(e,\nu)$ always lies in the range $0 \le m_T(e,\nu) \le m(e,\nu)$ and for $W \to e\nu$ decay, where $m(e,\nu) = M_W$, we have

$$0 \le m_T(e,\nu) \le M_W \tag{6.83}$$

- The m_T distribution for a given $\hat{s}$ is

$$\frac{d\hat{\sigma}}{dm_T^2} = \frac{\left|V_{qq'}\right|^2}{4\pi}\left(\frac{G_F M_W^2}{\sqrt{2}}\right)^2 \frac{1}{\left(\hat{s} - M_W^2\right)^2 + \left(\Gamma_W M_W\right)^2} \frac{2 - m_T^2/\hat{s}}{\sqrt{1 - m_T^2/\hat{s}}} \tag{6.84}$$

- The m_T distribution is unaffected by longitudinal boost of the $e\nu$ system, since it depends only on the transverse momenta

VI.8 Transverse Mass

- Boosting the e and ν momenta in a transverse direction, corresponding to a transverse velocity β of the decaying W boson, $m_T(e,\nu)$ is unchanged to order β and contains corrections only of order β^2

- Including the finite W width, convolving incident quark distributions and averaging color, the m_T distribution (at lowest order of the subprocess) becomes

$$\frac{d\sigma}{dm_T^2}\left(AB \to e\nu X\right) = \frac{K}{3}\sum_{q,q'}\int_0^1 dx_a \int_0^1 dx_b q(x_a,\hat{s})\bar{q}'(x_b,\hat{s})\frac{d\hat{\sigma}}{dm_T^2}\left(q\bar{q}' \to e\nu\right) \qquad (6.85)$$

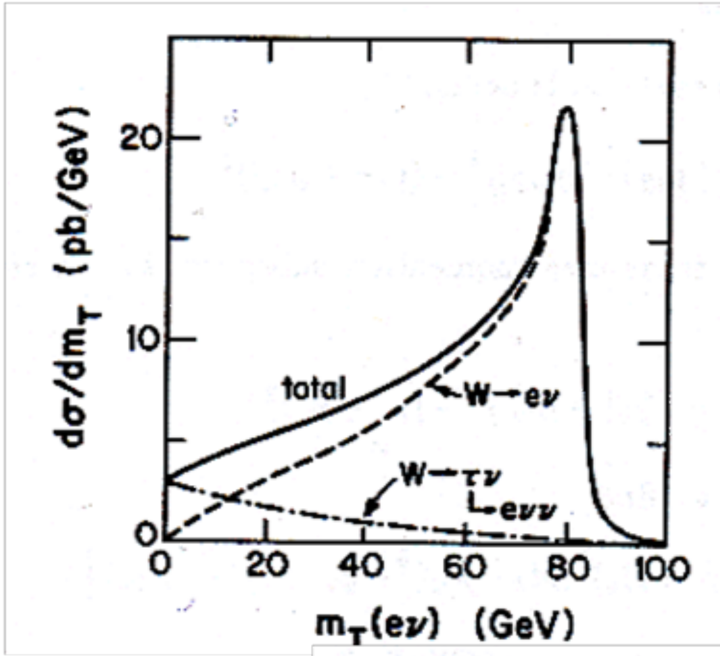

Fig. 8.11. Predicted distribution of transverse mass $m_T(e\nu)$ for $p\bar{p} \to W^\pm \to e\nu$ collisions at $\sqrt{s} = 630$ GeV.

with initial quark distribution evolved to $Q^2 = \hat{s}$ & the correction factor

$$K \simeq 1 + \frac{8\pi}{9}\alpha_s(M_W^2) \qquad (6.86)$$

VI.8 Transverse Mass

- The shape of the m_T distribution close to the endpoint is sensitive to both M_W & Γ_W
- The accuracy with which p^T_ν can be determined is a crucial limiting factor in determining the shape in this region
- For each event the uncertainty in $m_T(e, \nu)$ is $\Delta m_T \approx \Delta p^T_\nu$
- UA1 determined $M_W = 83 \pm 4$ GeV from the m_T distribution
- The curve is the theoretical calculation including acceptance and efficiency corrections
- A background to $W \to e\nu$ signal comes from the cascade decay $W \to \tau\nu$ with $\tau \to e\nu\bar{\nu}$
- Since the νs are undetected, this process is topologically indistinguishable from the signal

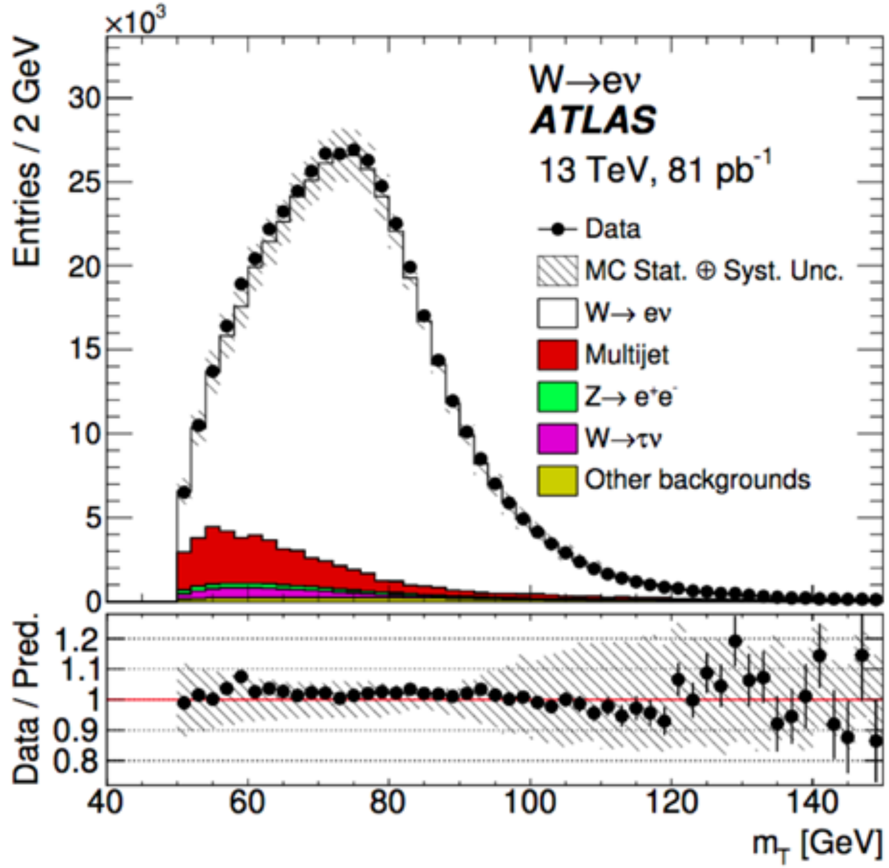

VI.8 Transverse Mass

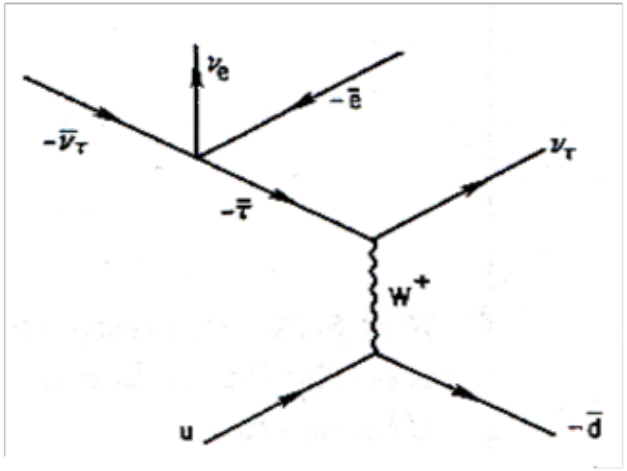

- The m_T distribution from $W\rightarrow\tau\rightarrow e$ mode is peaked towards low values wrt m_τ distribution from $W\rightarrow\nu e$

- New W-mass measurement from ATLAS

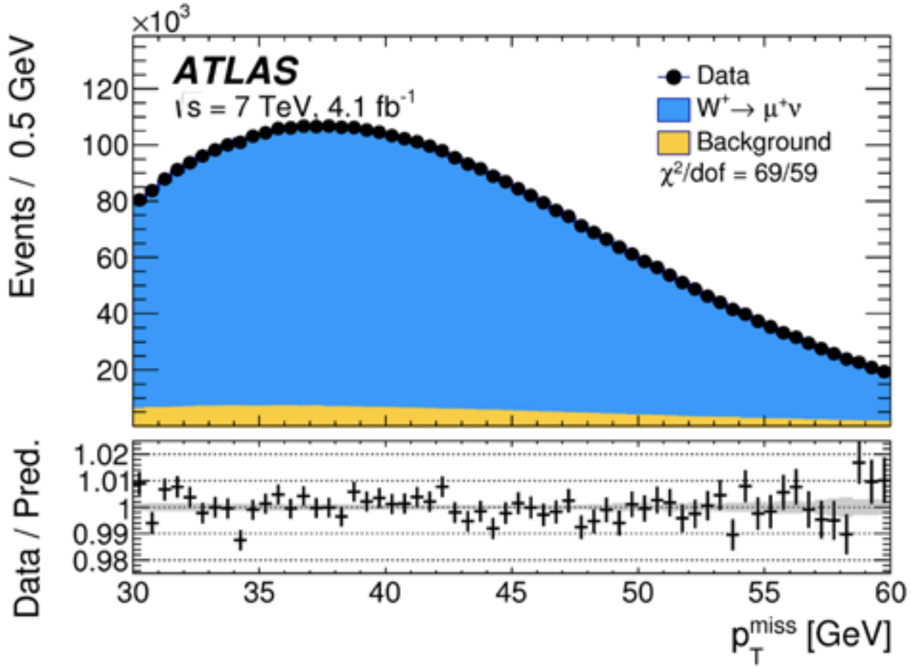

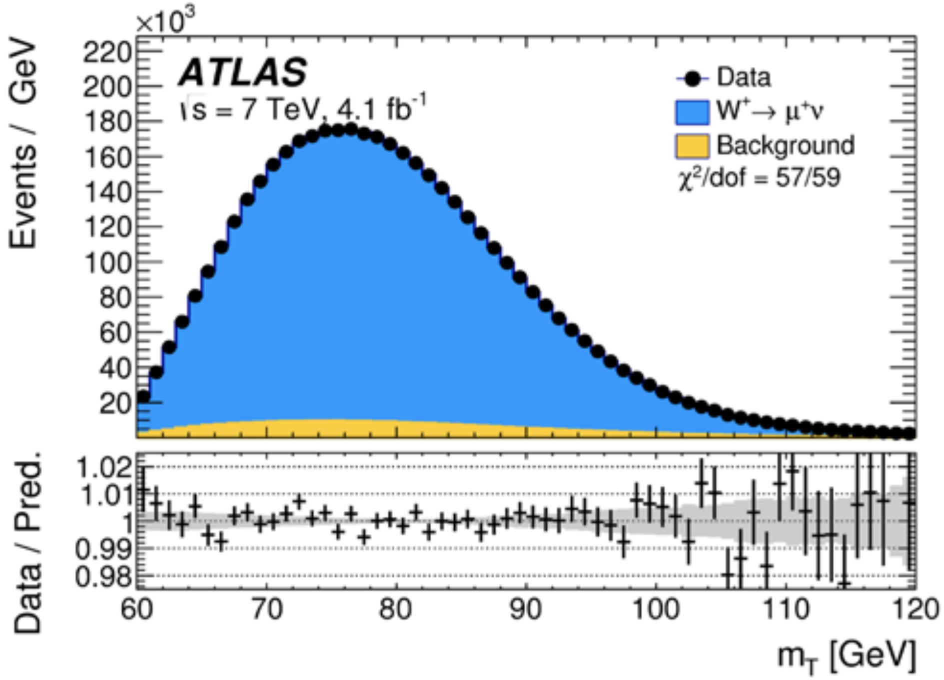

- Combining $e\nu$ and $\mu\nu$ channels yields

- This is the most precise single mass measurement

$$m_W = 80370 \pm 7_{stat} \pm 11_{sys} \pm 14_{Model} \text{ MeV} \qquad (6.87)$$

VI.8 Transverse Mass

❒ Comparison of W-mass measurements

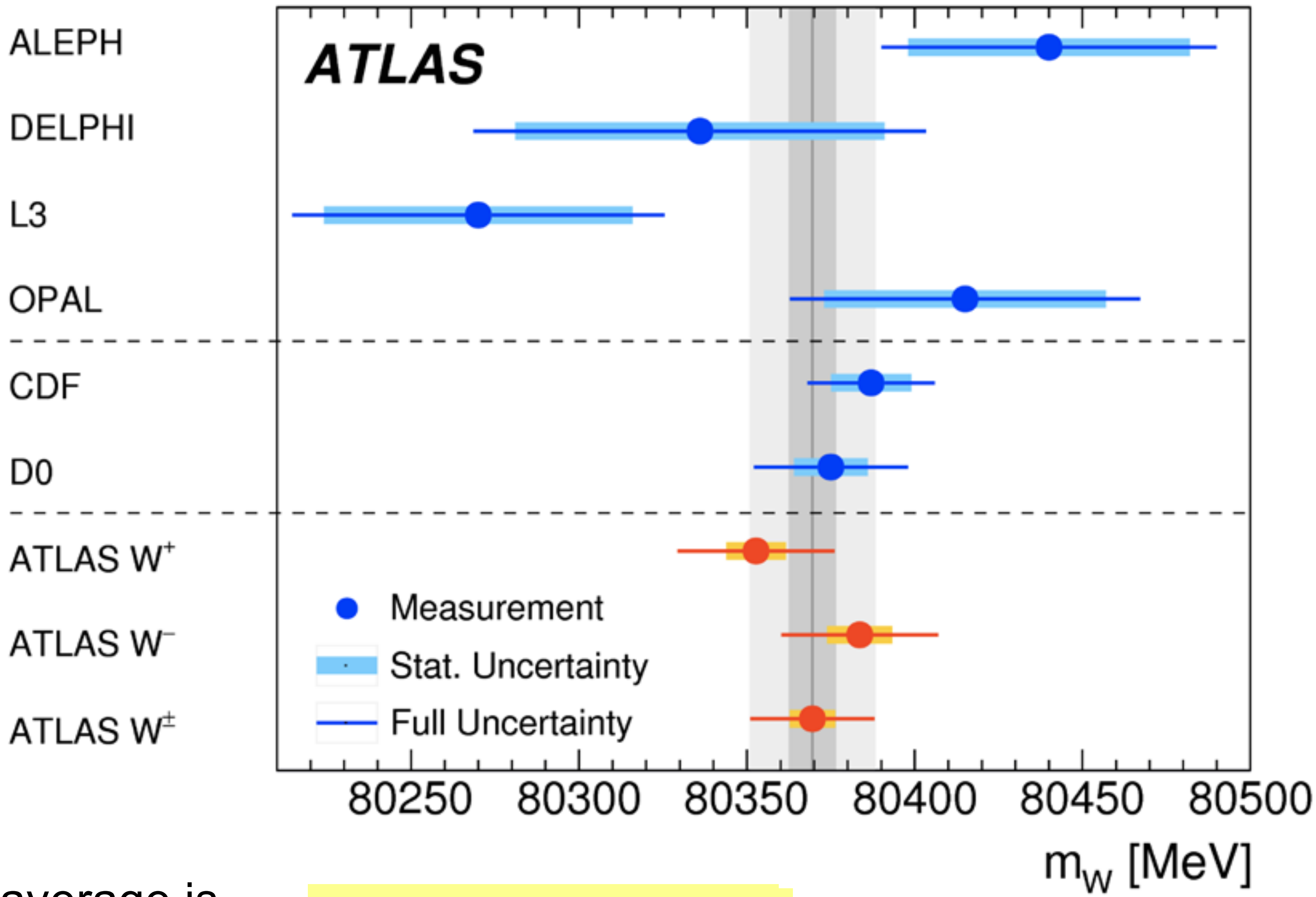

❒ Present world average is

$$m_W = 80385 \pm 15 \ MeV \tag{6.88}$$

VI.8 Transverse Mass

- ❒ SM consistency check, m_W vs m_t and m_H

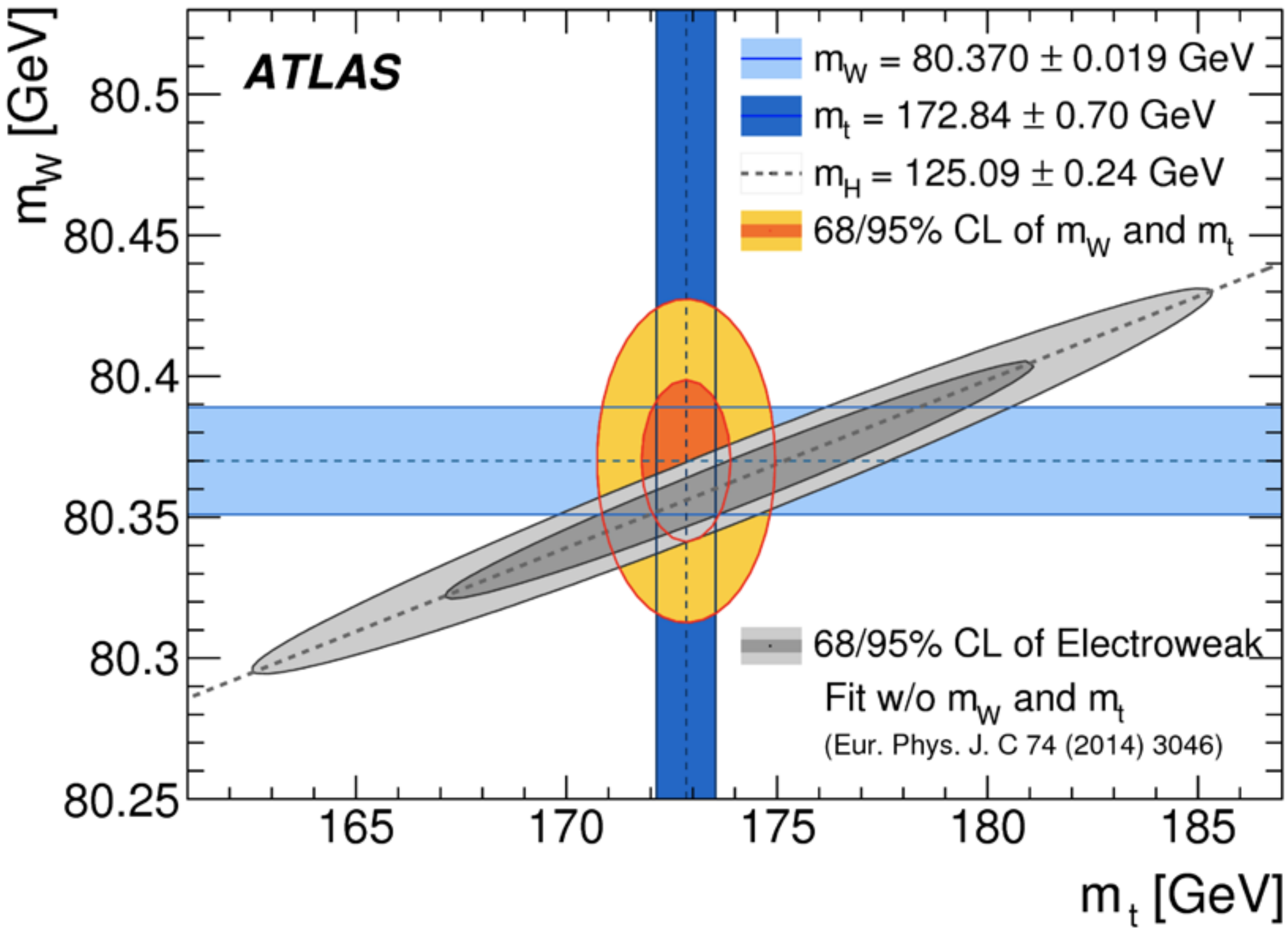

VI.9 Transverse Motion of the *W*

- The lowest-order fusion process $q\bar{q}' \rightarrow W$, evaluated with QCD-evolved quark distributions and multiplied by a *K*-factor for non-leading QCD corrections, gives the total *W* hadroproduction cross section correctly through order α_s

- The QCD-evolved quark distributions are given by the Alterelli-Parisi equations, that are differential equations for the quark & gluon evolutions

$$\frac{dq_i(x,Q^2)}{d(\ln Q^2)} = \frac{\alpha_s(Q^2)}{2\pi}\int_x^1 \frac{dw}{w}\left[q_i(w,Q^2)P_{qq}\left(\frac{x}{w}\right) + g((w,Q^2)P_{qg}\left(\frac{x}{w}\right)\right] \qquad (6.89)$$

$$\frac{dg(x,Q^2)}{d(\ln Q^2)} = \frac{\alpha_s(Q^2)}{2\pi}\int_x^1 \frac{dw}{w}\left[\sum_{q_i} q_i(w,Q^2)P_{gq}\left(\frac{x}{w}\right) + g((w,Q^2)P_{gg}\left(\frac{x}{w}\right)\right] \qquad (6.90)$$

- Here, *w* is the parton momentum fraction, *x* is the Bjorken variable $x=Q^2/(2P\bullet q)$ with Q^2 being the CMS energy squared, q is the momentum transfer and *P* is the momentum of the hadron containing the quark

- $q(w, Q^2)$ is the quark distribution, $g(w, Q^2)$ is the gluon distribution $P_{qq}(z)$, $P_{qg}(z)$, $P_{gq}(z)$ & $P_{gg}(z)$ are respectively the quark$\rightarrow$quark, quark$\rightarrow$gluon, gluon$\rightarrow$quark, gluon$\rightarrow$gluon splitting functions

VI.9 Transverse Motion of the *W*

- Introducing the prescription $1/(1-z)_t$ as

$$\int_0^1 dz \frac{h(z)}{(1-z)_t} \equiv \int_0^1 dz \frac{h(z)-h(1)}{(1-z)} \qquad (6.91)$$

which removes a singularity from $1/(1-z)$ expressing it as $\varepsilon^{-1}\delta(1-z)$ we can express the splitting functions by

$$P_{qq}(z) = \frac{4}{3}\frac{1+z^2}{(1-z)_t} + 2\delta(1-z) \qquad (6.92)$$

$$P_{qg}(z) = \frac{1}{2}\left[z^2(1-z)^2\right] \qquad (6.93)$$

$$P_{gq}(z) = \frac{4}{3}\frac{\left[1+(1-z)^2\right]}{z} \qquad (6.94)$$

$$P_{gg}(z) = 6\left[\frac{z}{(1-z)_t} + \frac{1-z}{z} + z(1-z) + \left(\frac{11}{12} - \frac{f}{18}\right)\delta(1-z)\right] \qquad (6.95)$$

where *f* is the # of quark flavors

- We also have the identities obtained by charge conjugation

$$P_{\bar{q}g}(z) = P_{qg}(z), \qquad P_{g\bar{q}}(z) = P_{gq}(z) \qquad (6.96)$$

VI.9 Transverse Motion of the *W*

- Momentum conservation at the splitting vertex yields

$$P_{qg}(z)=P_{qg}(1-z),\quad P_{gg}(z)=P_{gg}(1-z),\quad P_{qq}(z)=P_{qq}(1-z), \tag{6.97}$$

- The integral of $P_{qq}(z)$ over all z vanishes

$$\int_0^1 P_{qq}(z)dz=0 \tag{6.98}$$

while total momentum conservation implies

$$\int_0^1 dz\, z\left[P_{qq}(z)+P_{gq}(z)\right]=0 \tag{6.99}$$

$$\int_0^1 dz\, z\left[2fP_{qg}(z)+P_{gg}(z)\right]=0 \tag{6.100}$$

- Solving these equations by iteration will generate contributions to q of order $(\alpha_s \ln Q^2)^n$ from n-fold collinear gluon emission corresponding to graphs like

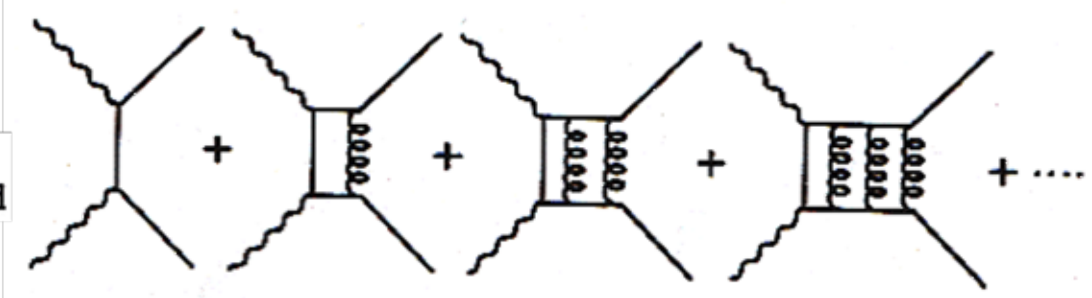

Fig. 7.7. The ladder graphs generated by repeated $q \to q$ splitting.

VI.9 Transverse Motion of the *W*

- A corresponding ladder of graphs arises from the solution of d$g(x,Q^2)$

- Since the Alterelli-Parisi equations are based on a longitudinal approximation, the QCD-evolved distributions do not include the transverse momentum that should accompany the radiation of gluons and quarks

- To include the p_T from radiated quarks & gluons, one can explicitly evaluate multiple emissions using techniques that sum radiated momenta and yield a net recoil W momentum

- An alternative is the use of MC simulations

- Consider a simplified approach based on the following subprocesses to order α_s

Fig. 8.14. $O(\alpha_s)$ annihilation and Compton subprocesses for W production.

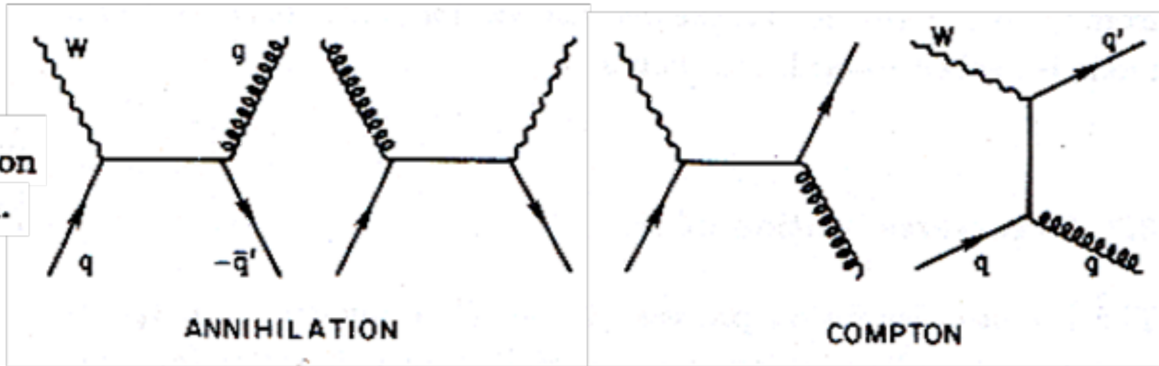

VI.9 Transverse Motion of the W

- The incident partons are evolved up to scale $Q^2=M^2_W$ in the convolution to obtain the hadronic cross sections

- At large p_T, these O(α_s) subprocesses are expected to dominate

- The argument of α_s is proportional to p^2_T and higher-order processes are suppressed by powers of α_s

- The spin-averaged and color-averaged cross section for the annihilation subprocess $q\bar{q}' \to Wg$ is

$$\frac{d\hat{\sigma}_{\mathrm{ann}}}{d\hat{t}} = \frac{4}{9}\alpha_s \frac{G_F M_W^2}{\sqrt{2}} \frac{\left|V_{qq'}\right|^2}{\hat{s}^2} \left[\frac{\hat{t}^2 + \hat{u}^2 + 2\hat{s}M_W^2}{\hat{t}\hat{u}}\right] \quad (6.101)$$

where $\hat{s} = (q+\bar{q}')^2,\ \hat{t} = (q-p_W)^2,\ \hat{u} = (\bar{q}-p_W)^2$

- Using crossing symmetry we can get the Compton subprocess $qg \to Wq'$

$$\frac{d\hat{\sigma}_{\mathrm{compton}}}{d\hat{t}} = \frac{1}{6}\alpha_s \frac{G_F M_W^2}{\sqrt{2}} \frac{\left|V_{qq'}\right|^2}{\hat{s}^2} \left[\frac{\hat{s}^2 + \hat{t}^2 + 2\hat{u}M_W^2}{-\hat{s}\hat{t}}\right] \quad (6.102)$$

VI.9 Transverse Motion of the W

- In pp collisions at $s^{1/2} < 1$ TeV $\sigma_{ann} \sim 10 \times \sigma_{compton}$ ➔ neglect $\sigma_{compton}$

- To get the distributions of $W \to e\nu$ decay products, we need ME for the complete production and decay sequence $q\bar{q}' \to Wg \to e\nu g$ containing W-polarization effects

- The differential cross section in a rather simple form is

$$d\sigma(\bar{u}d \to e\bar{\nu}g) = \left(\frac{G_F}{\sqrt{2}}\right)^2 \frac{32}{9\pi^4} \alpha_s \frac{M_W^4}{\hat{s}\hat{t}\hat{u}} |V_{ud}|^2 \left[\frac{(p_e \cdot p_{\bar{u}})^2 + (p_{\bar{\nu}} \cdot p_d)^2}{\left(p_W^2 - M_W^2\right)^2 + \Gamma_W^2 M_W^2}\right] \delta^4(p_{\bar{u}} + p_d - p_e - p_{\bar{\nu}} - p_g) \prod_{e,\bar{\nu},g} \frac{d^3 p_i}{2E_i} \qquad (6.103)$$

- The corresponding Compton formulas are again obtained by crossing

- These cross sections have mass and infrared singularities
  ➔ divergence at $p^2_T = 0$

- Infrared singularities cancel if loop diagrams are taken into account

VI.9 Transverse Motion of the W

- Mass singularities are factored out into the parton distributions
- This divergence is unphysical and would be explicitly removed in an ideal treatment
- Here, we simply regularize with a p_T cut-off factor (representing our ignorance of the precise details at small p_T) and multiply by the K-factor for non-leading enhancements
- The O(α_s) calculation already provides a useful approximation to the complete $AB\to WX$ hadronic production process if the cut-off factor is adjusted such that the integrated O(α_s) cross section equals to the total $AB\to WX$ cross section to order α_s

$$\int d_{ab} \int dp_T^2 f(p_T^2) d\sigma_1 \big/ dp_T^2 = \int d_{ab} K \sigma_0 \qquad (6.104)$$

where

$$d_{ab} = dx_a dx_b \sum_{q,q'} q(x_a, M_W^2) \bar{q}'(x_b, M_W^2) \qquad (6.105)$$

$d\sigma_1/dp_T^2$ is the O(α_s) $q\bar{q}' \to Wg$ differential cross section, $f(p_T^2)$ is the cut-off factor and σ_0 is the $q\bar{q}' \to W$ fusion cross section

VI.9 Transverse Motion of the *W*

- We have implicitly neglected the QCD enhancement of the first order cross section $d\sigma_1/dp_T^2$ that is known to be a resonance approximation

- Here the lowest-order cross section σ_0 enters only via the normalization condition

- This truncated QCD shower approximation is called "Poor Man's Shower Model" and gives both the total cross section and the p_T dependence at large p_T

- Note that it is not correct at small and intermediate p_T, but the integral is constrained to be correct

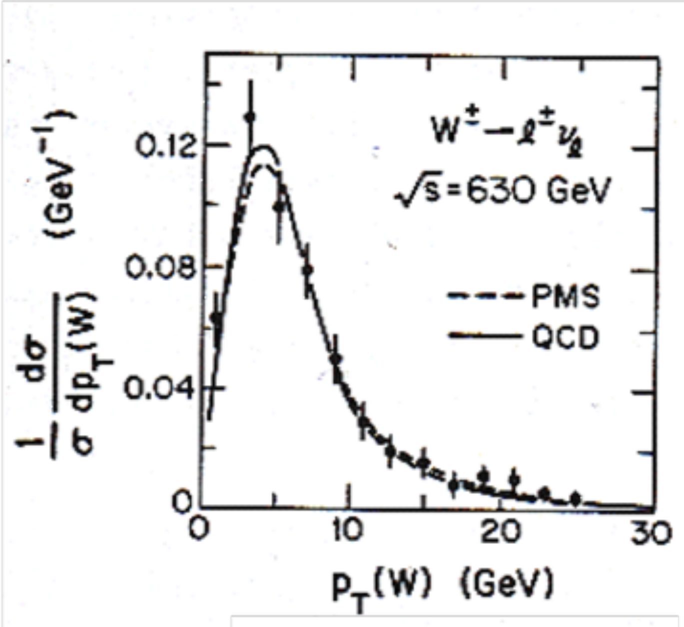

Fig. 8.15. Comparison of the truncated QCD shower prediction (PMS) and full QCD shower prediction with the $p_T(W)$ distribution measured by the UA1 collaboration at CERN $p\bar{p}$ collider.

VI.10 Weak Boson Decay Angular Distribution

- The *V-A* interaction causes e^- (e^+) from a W^- (W^+) decay to be emitted along the incoming quark (antiquark) with an angular distribution

$$d\hat{\sigma} / d\cos\hat{\theta} \sim \left(1+\cos\hat{\theta}\right)^2 \qquad (6.106)$$

where $\hat{\theta}$ is the emission angle of the e^- (e^+) wrt quark (antiquark) direction in the W rest frame

- The spin of the *W*-boson can be determined from the data using

$$\left\langle \cos\hat{\theta} \right\rangle = \left\langle \lambda \right\rangle \left\langle \mu \right\rangle / J(J+1) \qquad (6.107)$$

where $<\lambda>$ and $<\mu>$ are the global helicities of the system (ud) and decay system (eν), respectively

- For *V-A* interactions $<\lambda>=<\mu>=-1$ and J=1, yielding

$$\left\langle \cos\hat{\theta} \right\rangle = 0.5 \qquad (6.108)$$

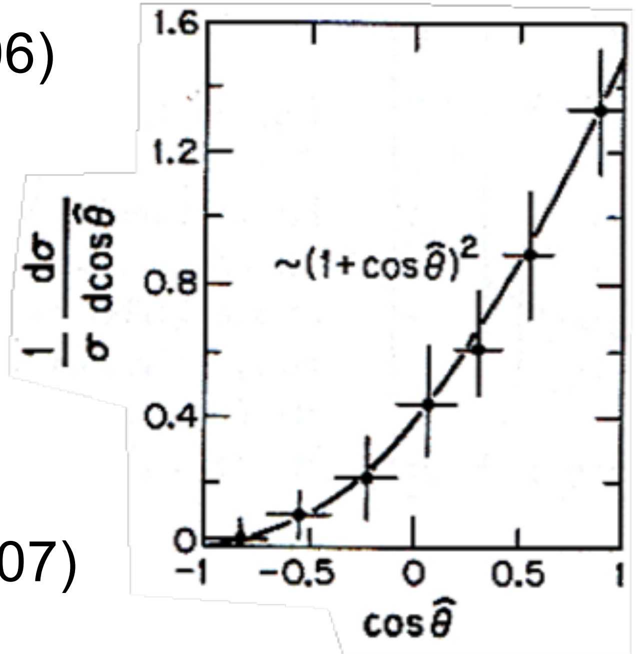

Fig. 8.16. Measured $W \to e\nu$ decay angular distribution from the UA1 collaboration at the CERN $p\bar{p}$ collider, compared with the predicted distribution for $V-A$ interactions.

VI.10 Weak Boson Decay Angular Distribution

while $\langle \cos\hat{\theta} \rangle = 0.0 \text{ for } J=0$ (6.109)

$\langle \cos\hat{\theta} \rangle \le 1/6 \text{ for } J=2$ (6.110)

- The experimental value of $\langle \cos\hat{\theta} \rangle = 0.43 \pm 0.07$ (6.111) agrees with the *J*=1 assignment for the *W*-boson and a prediction of maximal helicity at production and decay vertices

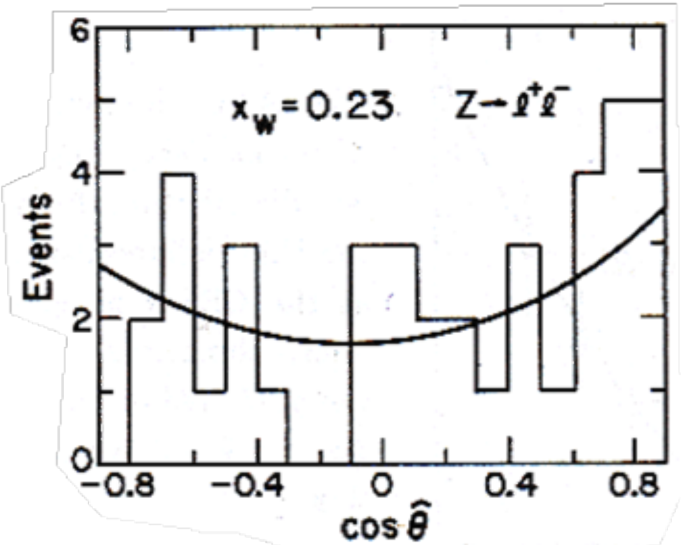

Fig. 8.17. Measured $Z \to \ell^+\ell^-$ decay angular distribution from the UA1 collaboration at the CERN $p\bar{p}$ collider, compared with standard model prediction for $x_W = 0.23$.

- Similar considerations apply to *Z* production and decay to e^+e^-

- The angular distributions here involve *V*-*A* and *V*+*A* couplings, which can be used to extract a value for x_W

- For $q\bar{q} \to Z^0 \to e^+e^-$ the angular distribution in the Z^0 rest frame is

$$\frac{d\hat{\sigma}}{d\cos\hat{\theta}} \sim \left[\left(g_V^q\right)^2 + \left(g_A^q\right)^2\right]\left[\left(g_V^e\right)^2 + \left(g_A^e\right)^2\right]\left(1+\cos^2\hat{\theta}\right) + 8 g_A^q g_V^q g_A^e g_V^e \cos\hat{\theta}$$

(6.112)

VI.11 *W* & *Z* Pair Production

- Production of $e^+e^- \to W^+W^-$ will yield a precise determination of the *W*-boson properties, such as mass, width and coupling to different flavors

- Furthermore, it provides the best opportunity to measure the $WW\gamma$ and *WWZ* couplings and test the gauge theory predictions for Yang-Mills self interactions

- There are cancellations among the 3 contributing diagrams ➔ small deviations from the gauge theory couplings would lead to observable effects

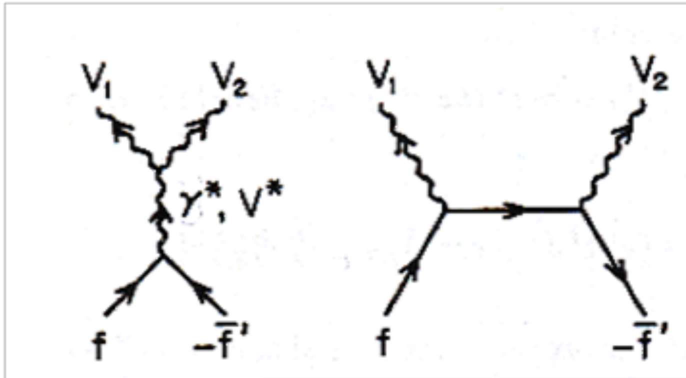

Fig. 8.18. Representative lowest order contributing diagrams for $f\bar{f}' \to V_1V_2$.

- In pp or p$\bar{\text{p}}$ collisions the W^+W^-, $W^{\pm}Z^0$ and Z^0Z^0 final states can be realized

- The W^+W^- contribution is an important background to the signal for a heavy Higgs boson, new heavy quarks & new heavy leptons

VI.11 *W* & *Z* Pair Production

- The amplitude for $f\bar{f}' \to V_1 V_2$ has the general form

$$M(f\bar{f}' \to V_1 V_2) = i\bar{v}(p_{f'})T^{\mu\nu}u(p_f)\varepsilon_\mu^*(p_{V_1})\varepsilon_\nu^*(p_{V_2}) \qquad (6.113)$$

where the ε terms denote the polarization vectors of the vector mesons and the tensor $T^{\mu\nu}$ is process dependent

- For the momenta we have used the notation

$$p_{\ell_1} = p_f - p_{V_1}, \quad p_{\ell_2} = p_f - p_{V_2} \qquad (6.114)$$

$$\hat{s} = (p_f + p_{f'})^2, \quad \hat{t} = p_{\ell_1}^2, \quad \hat{u} = p_{\ell_2}^2 \qquad (6.115)$$

and

$$D_V = \left(\hat{s} - M_V^2 + iM_V\Gamma_V\right)^{-1} \qquad (6.116)$$

The tensors for W^+W^-, Z^0Z^0 and $W^\pm Z^0$ production are given by

$$\begin{aligned} T_{\mu\nu}(W^+W^-) = {} & \underbrace{\overset{\gamma}{\boxed{e^2}}\left(\frac{Q_f}{\hat{s}} + \overset{Z^0}{\boxed{D_Z\frac{g_V^f - g_A^f\gamma_5}{x_W}}}\right)\left[g_{\mu\nu}\left(\not{p}_{V_1} - \not{p}_{V_2}\right) + \gamma_\mu\left(2p_{V_2} + p_{V_1}\right)_\nu - \gamma_\nu\left(2p_{V_1} + p_{V_2}\right)_\mu\right]}_{s\text{-channel}} \\ & - e^2\frac{(1+\gamma_5)}{4x_W}\left[\underbrace{\theta(-Q_f)\frac{\gamma_\mu\not{p}_{\ell_1}\gamma_\nu}{\hat{t}}}_{t\text{-channel}} + \underbrace{\theta(Q_f)\frac{\gamma_\mu\not{p}_{\ell_2}\gamma_\nu}{\hat{u}}}_{u\text{-channel}}\right] \end{aligned} \qquad (6.117)$$

VI.11 *W* & *Z* Pair Production

$$T_{\mu\nu}(Z^0Z^0) = -e^2 \frac{\left(g_V^f\right)^2 + \left(g_A^f\right)^2 - 2g_V^f g_A^f \gamma_5}{x_W(1-x_W)} \left[\underbrace{\frac{\gamma_\mu \not{p}_{\ell_1} \gamma_\nu}{\hat{t}}}_{t} + \underbrace{\frac{\gamma_\mu \not{p}_{\ell_2} \gamma_\nu}{\hat{u}}}_{u} \right] \tag{6.118}$$

$$T_{\mu\nu}(W^-Z^0) = e^2 \frac{V_{ff'}(1+\gamma_5)}{2\sqrt{2}x_W \cos\theta_W} \left\{ \underbrace{D_W(1-x_W)\left[g_{\mu\nu}\left(\not{p}_Z - \not{p}_W\right) + \gamma_\nu(2p_W + p_Z)_\mu - \gamma_\mu(2p_Z + p_W)_\nu \right]}_{s} - g_L^f \underbrace{\frac{\gamma_\mu \not{p}_{\ell_1} \gamma_\nu}{\hat{t}}}_{t} - g_L^{f'} \underbrace{\frac{\gamma_\mu \not{p}_{\ell_2} \gamma_\nu}{\hat{u}}}_{u} \right\} \tag{6.119}$$

- For W^+Z^0 production we need to interchange g^f and $-g^{f'}$ as well as interchange $\hat{u}$ and $\hat{t}$ in the W^-Z^0 expression above
- To express the differential cross section we introduce the notation

$$U_T = \hat{u}\hat{t} - M_{V_1}^2 M_{V_2}^2 \tag{6.120}$$

$$\beta_V = \sqrt{\left[\left(1-\left(M_{V_1}^2 + M_{V_2}^2\right)/\hat{s}\right)^2 - 4M_{V_1}^2 M_{V_2}^2/\hat{s}^2\right]} \quad \text{threshold factor} \tag{6.121}$$

- We also need a color factor C (C=1/3for $q\bar{q}$ & C=1 for e^+e^-) and 3rd component of the weak isospin T^f_3

VI.11 *W* & *Z* Pair Production

- The cross section for W^+W^- is

$$\frac{d\hat{\sigma}(W^+W^-)}{d\hat{t}} = \frac{\pi\alpha^2 C}{4x_W^2\hat{s}^2}\Bigg\{\underbrace{\frac{U_t}{\hat{s}^2}}_{\gamma}\Bigg[3 - \underbrace{\frac{1}{1-x_W}\frac{g_L^f}{T_3^f}\left(\hat{s}-6M_W^2\right)\Re e D_Z}_{\gamma\text{-}Z^0} + \underbrace{\frac{\left(g_L^f\right)^2+\left(g_R^f\right)^2}{\left(1-x_W\right)^2}\left(\beta_W+\frac{12M_W^4}{\hat{s}^2}\right)\hat{s}^2\left|D_Z\right|^2}_{Z^0}\Bigg]$$

s-channel

(mass term)

$$-\frac{4g_L^f}{T_3^f}M_Z^2\Re e D_Z \qquad +4\frac{\left(g_L^f\right)^2+\left(g_R^f\right)^2}{1-x_W}M_Z^2\hat{s}\beta_W^2\left|D_Z\right|^2$$

$$+\theta(-Q_f)\left[2\left(1+\frac{g_L^f}{T_3^f}M_Z^2\Re e D_Z\right)\times\left(\frac{U_T}{\hat{s}\hat{t}}-\frac{2M_W^2}{\hat{t}}\right)+\frac{U_T}{\hat{t}^2}\right] \quad t\text{-channel}$$

$$+\theta(Q_f)\left[2\left(1+\frac{g_L^f}{T_3^f}M_Z^2\Re e D_Z\right)\times\underbrace{\left(\frac{U_T}{\hat{s}\hat{u}}-\frac{2M_W^2}{\hat{u}}\right)}_{s\text{-}u\text{ interference}}+\frac{U_T}{\hat{u}^2}\right]\Bigg\} \quad u\text{-channel}$$

(6.122)

s-*t* interference

VI.11 W & Z Pair Production

- The cross section for Z^0Z^0 is

$$\frac{d\hat{\sigma}(Z^0Z^0)}{d\hat{t}} = \frac{\pi\alpha^2 C}{x_W^2\hat{s}^2}\frac{\left(g_L^f\right)^4+\left(g_R^f\right)^4}{(1-x_W)^2}\left[\frac{\hat{t}}{\hat{u}}+\frac{\hat{u}}{\hat{t}}+\frac{4M_Z^2\hat{s}}{\hat{t}\hat{u}}-M_Z^4\left(\frac{1}{\hat{t}^2}+\frac{1}{\hat{u}^2}\right)\right] \tag{6.123}$$

- Since both Z^0 are indistinguishable, t and u channels are symmetric and interfere

- The cross section for W^-Z^0 is

$$\begin{aligned}\frac{d\hat{\sigma}(W^-Z^0)}{d\hat{t}} = \frac{\pi\alpha^2 C\left|V_{ff'}\right|^2}{2x_W^2\hat{s}^2}\Bigg\{&\left[\frac{1}{4}\left[(9-8x_W)U_T-(6-8x_W)\left(M_W^2+M_Z^2\right)\hat{s}\right]\left|D_W\right|^2\right. && \Big\}\ s \text{ channel}\\ &+2\left[U_T-\left(M_W^2+M_Z^2\right)\hat{s}\right]\times\left(\frac{\left(g_L^f\right)^2}{\hat{t}}-\frac{\left(g_L^f\right)^2}{\hat{u}}\right)\Re e D_W && \Big\}\ \begin{matrix} s\text{-}t \\ s\text{-}u\end{matrix}\\ &+\frac{U_T}{1-x_W}\left(\underbrace{\frac{\left(g_L^f\right)^2}{\hat{t}}}_{t}+\underbrace{\frac{\left(g_L^f\right)^2}{\hat{u}}}_{u}\right)+2\frac{\left(M_W^2+M_Z^2\right)\hat{s}}{1-x_W}\underbrace{\frac{g_L^f}{\hat{t}}\frac{g_L^f}{\hat{u}}}_{t\text{-}u \text{ interference}}\Bigg\}\end{aligned} \tag{6.124}$$

VI.11 *W* & *Z* Pair Production

- For W^+Z^0 production we just need to interchange $\hat{t} \leftrightarrow \hat{u}$

- The energy dependence of total cross section is crucially dependent on gauge cancellations

- For example, in $e^+e^-\to W^+W^-$ the contribution of the ν exchange diagram grows rapidly with energy

$$\sigma(\nu-\text{exchange}) \simeq \frac{\pi\alpha^2 s}{96 x_W^2 M_W^4} \qquad (6.125)$$

whereas

$$\sigma_{SM} \simeq \frac{\pi\alpha^2}{2x_W^2 s}\ln\left(\frac{s}{M_W^2}\right) \qquad (6.126)$$

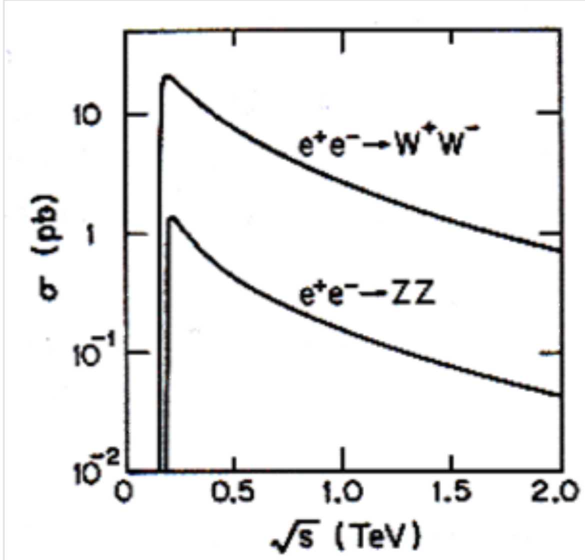

Fig. 8.19. Total cross sections for $e^+e^- \to W^+W^-$ and ZZ versus the total c.m. energy $\sqrt{s}$.

- In $e^+e^-\to W^+W^-$, the W^+ is preferentially produced along e^+ direction

- The energy distribution is more sharply peaked as $s^{1/2}$ increases

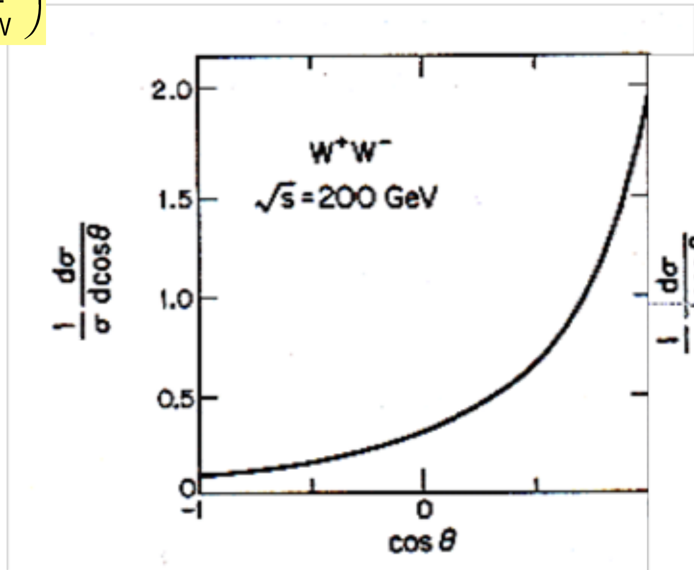

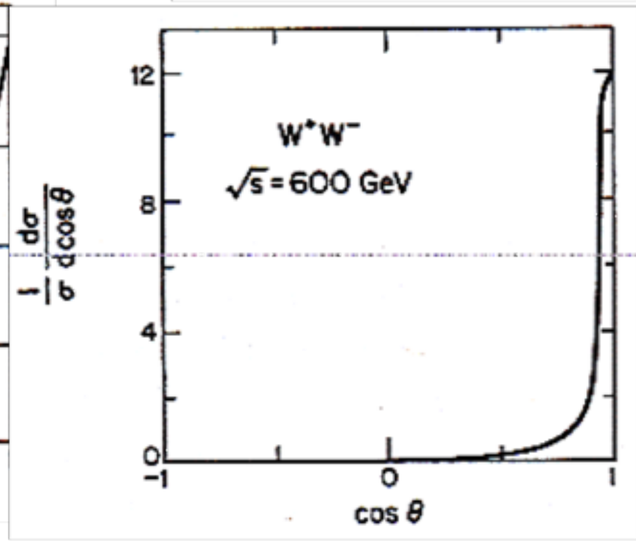

VI.11 *W* & *Z* Pair Production

- This will enable us to separate off contributions from new physics sources that decay to W^+W^- (Higgs, heavy lepton, heavy quark)
- In $e^+e^- \to W^+W^-$ production boson spins are correlated ➔ yields correlation between their decay products $W^+ \to a\bar{b}$, $W^- \to c\bar{d}$, where a,b,c,d are leptons or quarks (jets)
- To calculate these effects the full *ME* for $e^+e^- \to a\bar{b}c\bar{d}$ must be evaluated
- There are many lepton-lepton, lepton-quark, quark-quark correlations that can be studied to test the gauge theory couplings
- The WZ production process has a clean experimental signature with $W^+ \to e^+\nu$ & $Z \to e^+e^-$

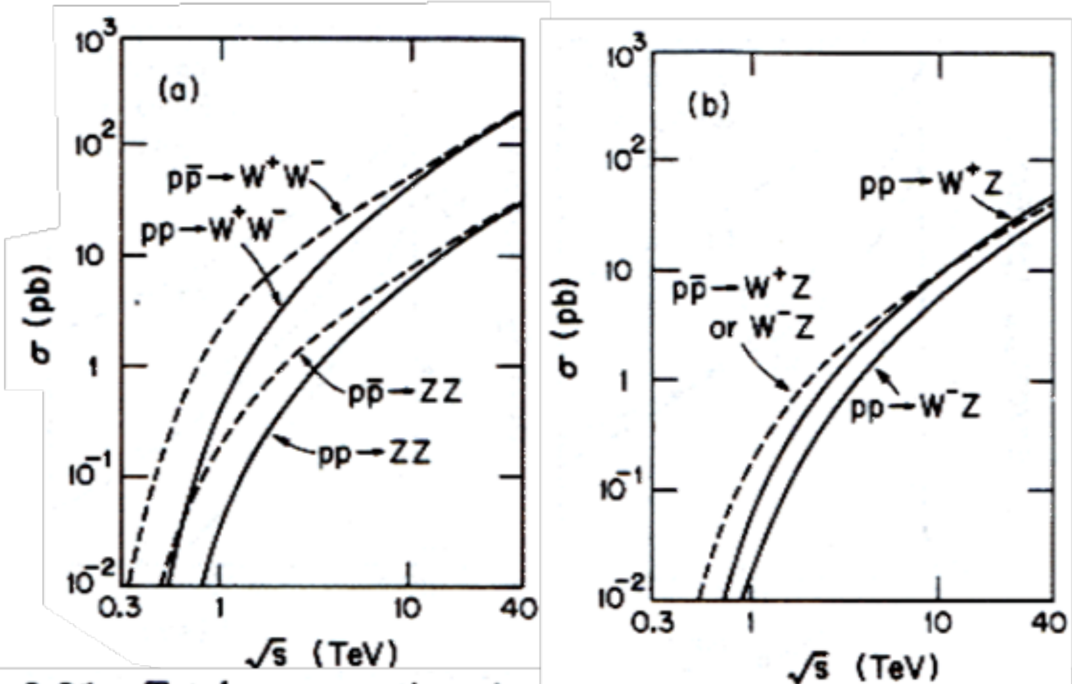

Fig. 8.21. Total cross sections in pp and $p\bar{p}$ collisions for gauge boson pair production versus the total energy $\sqrt{s}$: (a) W^+W^- and ZZ; (b) $W^\pm Z$.

$s^{1/2}$=1.96 TeV

$$CDF : \sigma(p\bar{p} \to WZ) = (4.1 \pm 0.7)\text{pb} \quad (6.127)$$

$$CDF : \sigma(p\bar{p} \to ZZ) = (1.7^{+1.2}_{-0.7} \pm 0.2)\text{pb} \quad (6.128)$$

VI.11 *W* & *Z* Pair Production

❒ ATLAS measurements are in good agreement with NNLO predictions

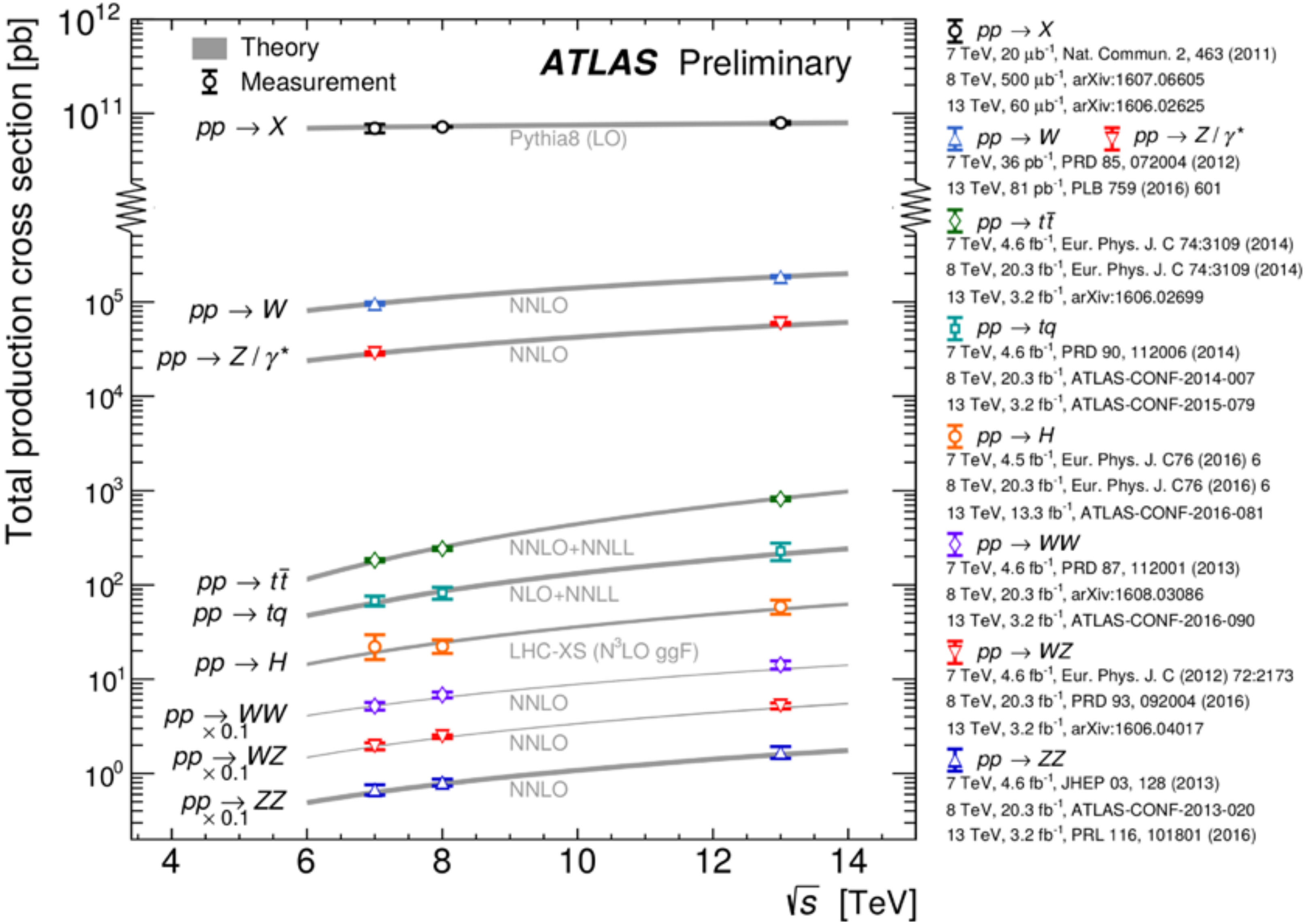

VI.11 *W* & *Z* Pair Production

- The *W* and *Z* pair cross sections for transversely & Longitudinally polarized vector bosons have also been evaluated
- At high $s^{1/2} \gg M_W$, the cross sections for transversely-polarized *W* and *Z* bosons dominates over those for longitudinal polarizations

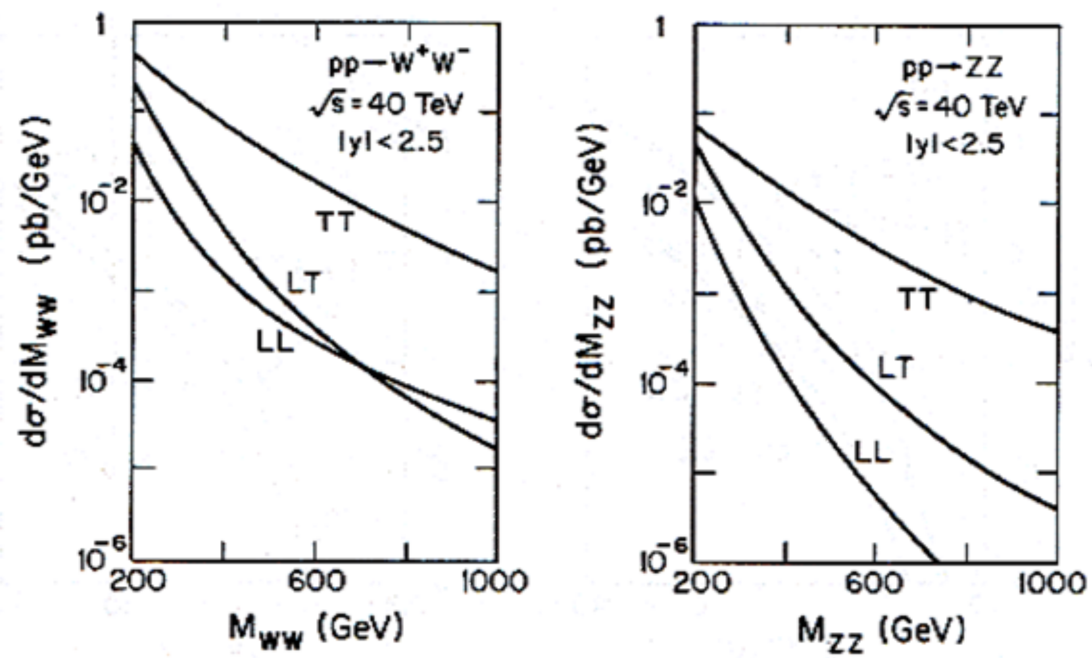

Fig. 8.22. Invariant mass distribution for W^+W^- and ZZ pair production in pp collisions at 40 TeV. T (transverse) and L (longitudinal) refer to the polarizations of the weak bosons.

VI.11 *W* & *Z* Pair Production

- The Goldstone-boson equivalence theorem states that the amplitude involving longitudinally-polarized gauge bosons is equivalent to the amplitude with external gauge bosons replaced by corresponding Goldstone bosons up to corrections of order M_V/E_V, where E_V is the gauge boson energy

- The couplings of Goldstone bosons are like those of the physical Higgs boson, since they belong to the original SU(2) Higgs doublet ➔ the coupling of longitudinally-polarized W & Z bosons to light quarks is at high energies by a factor of ~ M_V/E_V

- On the other hand, *W* & *Z* bosons that result from the decay of heavy particles are predominantly longitudinally polarized

- For example the couplings of Goldstone boson pairs to *H*, *Z*' & a heavy quark are enhanced by factors of $(m_H/M_W)^2$, $(m_{Z'}/M_W)^2$, and $(m_f/M_W)^2$, respectively ➔this helps to separate these signals from continuum backgrounds

VI.11 *W* & *Z* Pair Production

- In order to observe *VV* production we encounter 3 topologies for *WW* final states:

  - $WW \to 4q$: 45.7% ➔ 4 jets
  - $WW \to 2q\ell\nu$: 43.8% ➔ 2 jets + 1 ch lepton + missing energy
  - $WW \to \ell\nu\ell\nu$: 10.5% ➔ 2 ch leptons + missing energy

- For *ZZ* final states we encounter 6 different topologies

  - $ZZ \to 4q$: 49.0% ➔ 4 jets
  - $ZZ \to 2q\nu\bar{\nu}$: 28.0% ➔ 2 jets + missing energy
  - $ZZ \to 2q\ell^+\ell^-$: 14.0% ➔ 2 jets + 2 ch leptons
  - $ZZ \to \ell^+\ell^-\nu\bar{\nu}$: 4.0% ➔ 2 ch leptons + missing energy
  - $ZZ \to 2\ell^+\ell^-$: 1.0% ➔ 4 ch leptons
  - $ZZ \to 2\nu\bar{\nu}$: 4.0% ➔ missing energy (not seen)

VI.11 *W* & *Z* Pair Production

- The $e^+e^- \to W^+W^-$ cross section has been measure at LEP II

- The measurements are in excellent agreement with the SM prediction

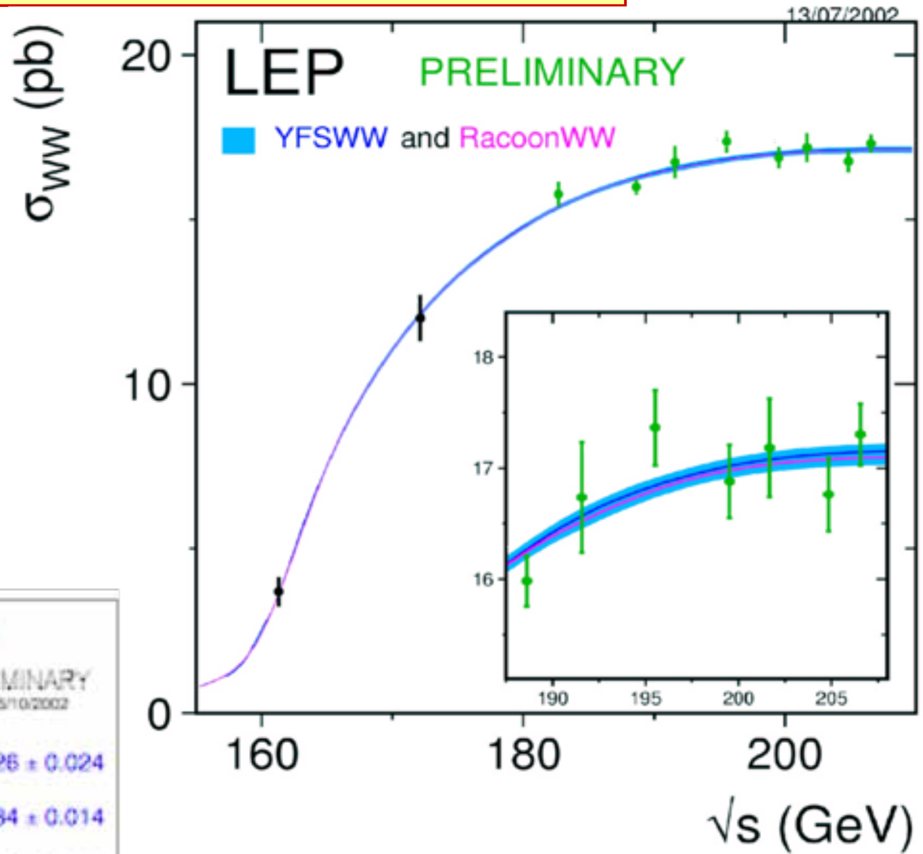

Measurements of W-pair cross section vs energy in comparison to 2 predictions. The shaded band shows theoretical uncertainties, ranging from 0.7% to 0.4% above $s^{1/2}$>170 GeV & 2% below.

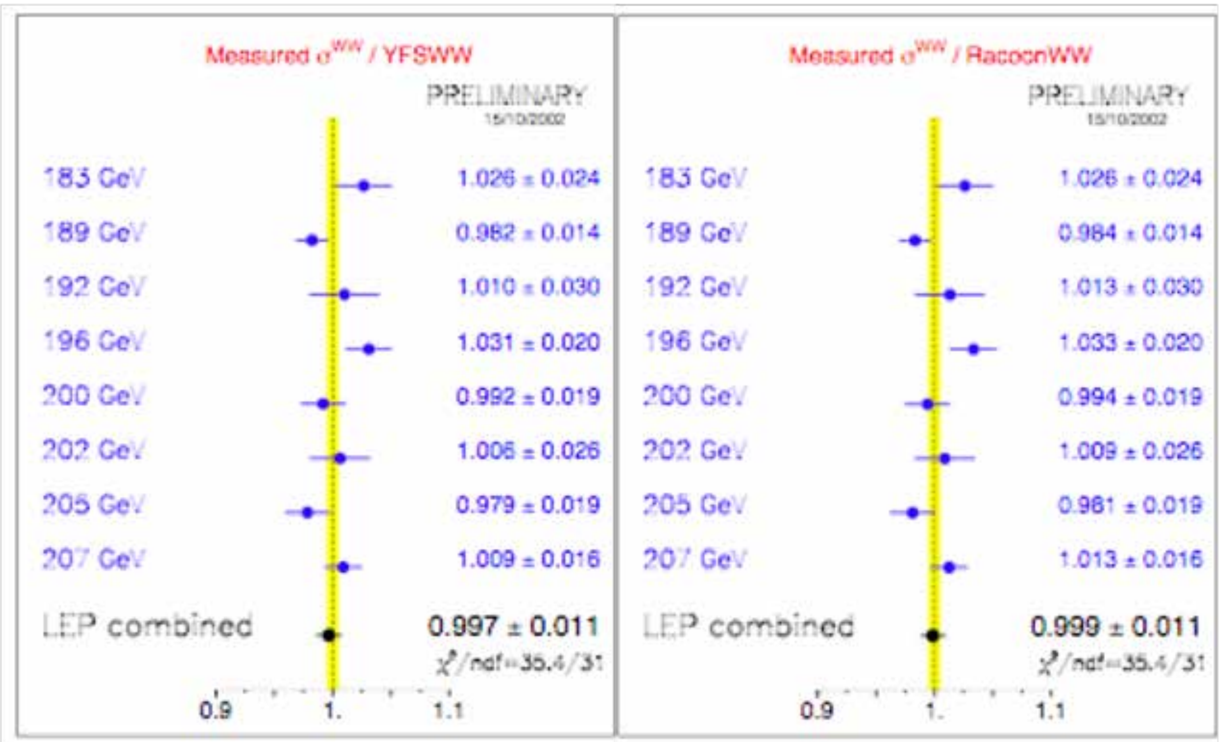

Ratios of LEP-combined W pair cross section measurements for different energies to 2 predictions. The yellow band shows a 0.5% theoretical error between the 2 predictions

VI.11 *W* & *Z* Pair Production

- The $e^+e^- \to Z^0Z^0$ cross section has been measure at LEP II

- The measurements are in excellent agreement with the SM prediction

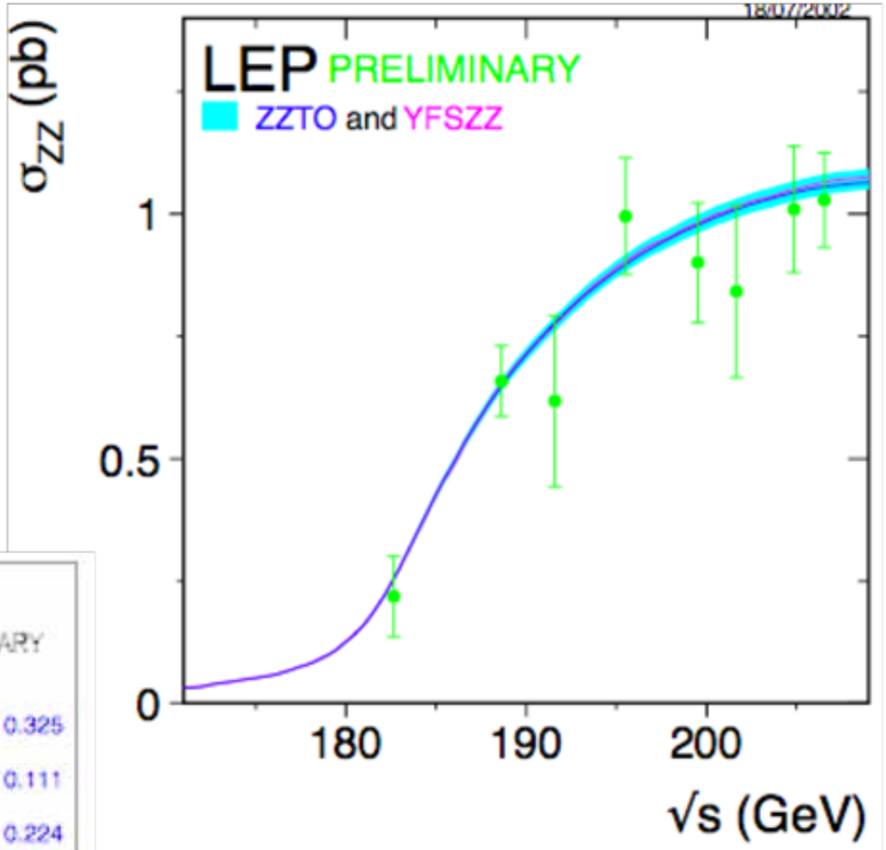

Measurements of Z-pair cross section vs energy in comparison to 2 predictions. The shaded band shows theoretical uncertainty of 2%.

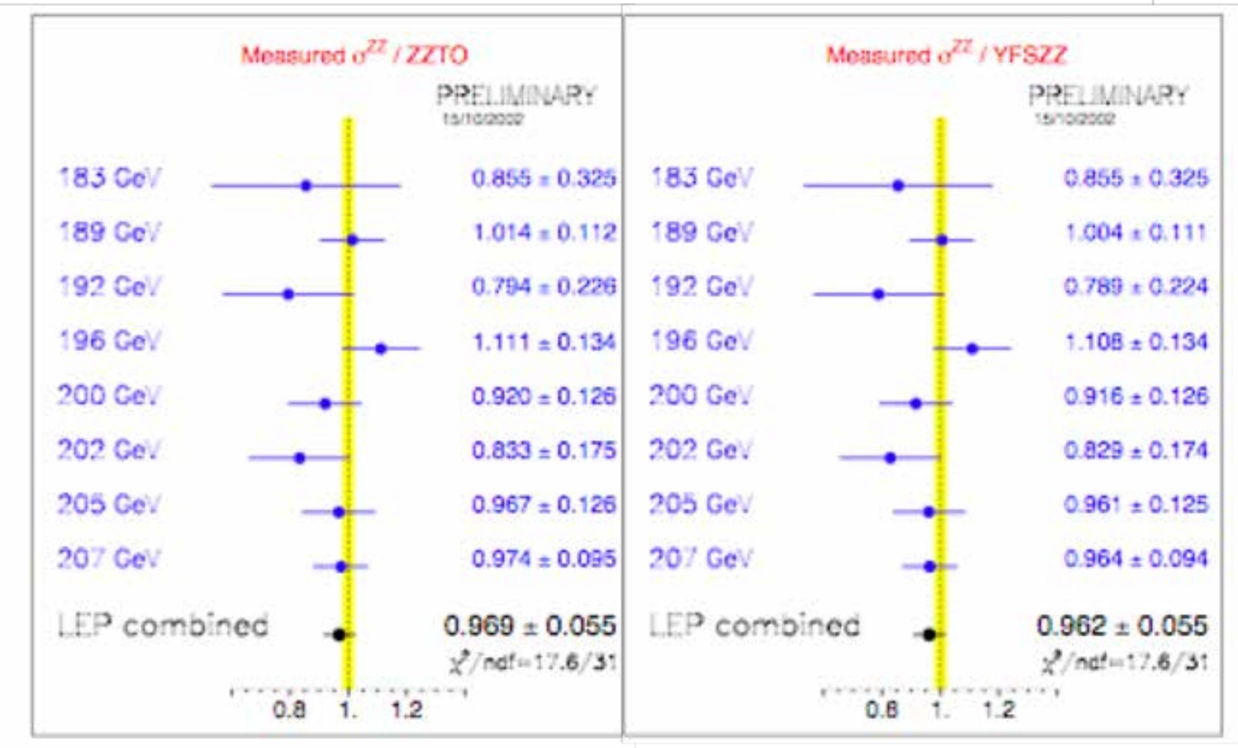

Ratios of LEP-combined Z pair cross section measurements for different energies to 2 predictions. The yellow band shows a 2% theoretical error between the 2 predictions

VI.12 Tripple Gauge Couplings

- In the SM 3 or 4 gauge bosons can couple to each other, which is a consequence of the non-Abelean group SU(2)$\times$U(1)

- The most general Lorentz-invariant Lagrangian that describes triple gauge-boson interactions has 14 independent complex couplings, 7 for $WW\gamma$ vertex and 7 for WWZ vertex

- Assuming EM gauge invariance as well as C & P conservation, the # of independent TGC reduces to 5 ➔ common set $\{g_1^Z, \kappa_Z, \kappa_\gamma, \lambda_Z, \lambda_\gamma\}$; $(g_1^\gamma = 1)$

$$\mathcal{L} = ig_{WWV}\left[g_1^V\left(W^+_{\mu\nu}W^{-\mu} - W^{+\mu}W^-_{\mu\nu}\right)V^\nu + \boldsymbol{\kappa}^V W^+_\mu W^-_\nu V^{\mu\nu} + \frac{\lambda^V}{m_W^2}W^{+\nu}_\mu W^{-\rho}_\nu V^\mu_\rho\right] \qquad \begin{aligned} g_{WW\gamma} &= e \\ g_{WWZ} &= e \bullet \cot\boldsymbol{\theta}_W \end{aligned} \qquad (6.129)$$

- In the SM we expect $g_1^Z = \kappa_Z = \kappa_\gamma = 1$ and $\lambda_Z = \lambda_\gamma = 0$;

- The LEP experiments used g_1^Z, κ_γ, λ_γ with the gauge constraint

$$\kappa_Z = g_1^Z - (\kappa_\gamma - 1)\tan^2\theta_W \qquad \& \qquad \lambda_Z = \lambda_\gamma \qquad (6.130)$$

where all couplings are considered real

- The neutral TGC (ZZγ, ZZZ) are described by the parameters h^V_i, i=1..4, & f^V_j, j=4,5, assumed to be real & vanishing in the SM ($V=\gamma$, Z)

VI.12 Tripple Gauge Couplings

❐ The LEP results for charged TGC are consistent with the SM

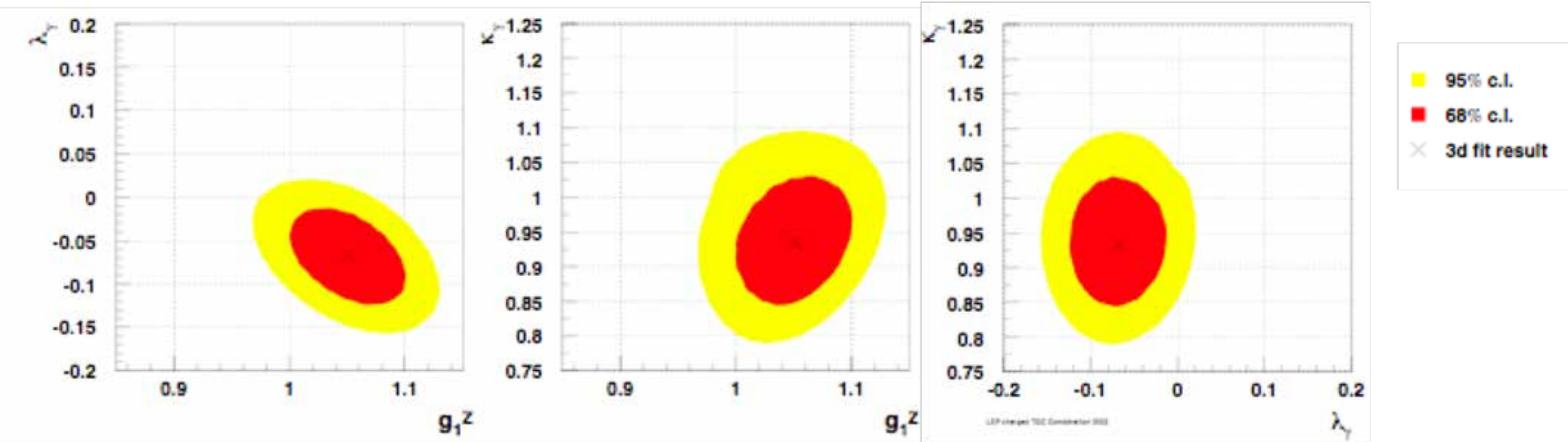

$$g_1^Z = 1.051^{+0.031}_{-0.032} \qquad \kappa_Z = 0.933^{+0.051}_{-0.059} \qquad \lambda_\gamma = -0.067^{+0.036}_{-0.038} \qquad (6.131)$$

❐ Similarly, the results for the neutral TGC are consistent with zero and thus in good accord with the SM

❐ New gauge bosons would contribute to this coupling & modify the SM values ➔ need precision measurements to detect new physics